



UNIVERSITY OF LEEDS

This is a repository copy of *Deformation–sedimentation feedback and the development of anomalously thick aggradational turbidite lobes: Outcrop and subsurface examples from the Hikurangi Margin, New Zealand*.

White Rose Research Online URL for this paper:
<http://eprints.whiterose.ac.uk/171030/>

Version: Accepted Version

Article:

McArthur, AD orcid.org/0000-0002-7245-9465, Bailleul, J, Mahieux, G et al. (3 more authors) (2021) Deformation–sedimentation feedback and the development of anomalously thick aggradational turbidite lobes: Outcrop and subsurface examples from the Hikurangi Margin, New Zealand. *Journal of Sedimentary Research*, 91 (4). pp. 362-389. ISSN 1527-1404

<https://doi.org/10.2110/jsr.2020.013>

This item is protected by copyright. This is an author produced version of an article published in *Journal of Sedimentary Research*. Uploaded in accordance with the publisher's self-archiving policy.

Reuse

Items deposited in White Rose Research Online are protected by copyright, with all rights reserved unless indicated otherwise. They may be downloaded and/or printed for private study, or other acts as permitted by national copyright laws. The publisher or other rights holders may allow further reproduction and re-use of the full text version. This is indicated by the licence information on the White Rose Research Online record for the item.

Takedown

If you consider content in White Rose Research Online to be in breach of UK law, please notify us by emailing eprints@whiterose.ac.uk including the URL of the record and the reason for the withdrawal request.



eprints@whiterose.ac.uk
<https://eprints.whiterose.ac.uk/>

1 Deformation-sedimentation feedback and the development of
2 anomalously thick aggradational turbidite lobes: outcrop and
3 subsurface examples from the Hikurangi Margin, New Zealand

4 McArthur, A.D.^{1*}, Bailleul, J.², Mahieux, G.³, Claussmann, B.^{2,4}, Wunderlich, A.⁵,
5 McCaffrey, W.D.¹

6 1. School of Earth and Environment, University of Leeds, Leeds, LS2 9JT, United
7 Kingdom

8 2. U2R 7511, Basins-Reservoirs-Resources (B2R), Geosciences department,
9 UniLaSalle, 60026, Beauvais, France

10 3. U2R 7511, Basins-Reservoirs-Resources (B2R), Université de Picardie Jules Verne,
11 80039, Amiens, France

12 4. Schlumberger, Software Integrated Solutions, London, SW1E 6AJ, United Kingdom

13 5. OMV New Zealand Ltd, The Majestic Centre, 100 Willis Street, 6011 Wellington,
14 New Zealand

15 * Email: a.mcarthur@leeds.ac.uk

16 **ABSTRACT**

17 Concepts of the interaction between autogenic (e.g., flow process) and allogenic (e.g.,
18 tectonics) controls on sedimentation have advanced to a state that allows the controlling
19 forces to be distinguished. Here we examine outcropping and subsurface Neogene deep-
20 marine clastic systems that traversed the Hikurangi subduction margin via thrust-bounded
21 trench-slope basins, providing an opportunity to examine the interplay of structural

22 deformation and deep-marine sedimentation. Sedimentary logging and mapping of Miocene
23 outcrops from the exhumed portion of the subduction wedge record heavily amalgamated,
24 sand-rich lobe complexes, up to 200 m thick, which accumulated behind NE-SW orientated
25 growth structures. There was no significant deposition from low-density parts of the gravity-
26 flows in the basin centre, although lateral fringes demonstrate fining and thinning indicative
27 of low-density flow deposits. Seismic data from the offshore portion of the margin show
28 analogous lobate reflector geometries. These deposits accumulate into complexes up to 5 km
29 wide, 8 km long and 300 m thick, comparable in scale with the outcropping lobes on this
30 margin. Mapping reveals lobe complexes that are vertically stacked behind thrusts. These
31 results illustrate repeated trapping of the sandier parts of turbidity currents to form
32 aggradational lobe complexes, with the finer-grained suspended load bypassing to areas
33 downstream. However, the repeated development of lobes characterised by partial bypass
34 implies that a feedback mechanism operates to perpetuate a partial confinement condition, via
35 rejuvenation of accommodation. The mechanism proposed is a coupling of sediment loading
36 and deformation rate, such that load-driven subsidence focuses stress on basin bounding
37 faults and perpetuates generation of accommodation in the basin, hence modulating tectonic
38 forcing. Recognition of such a mechanism has implications for understanding the tectono-
39 stratigraphic evolution of deep-marine fold and thrust belts and the distribution of resources
40 within them.

41 **Keywords:** lobe complexes; Neogene; deep-marine; trench-slope basin; tectono-
42 stratigraphic; feedback mechanism

43 INTRODUCTION

44 Understanding the interaction between autogenic and allogenic controls is a current
45 research focus in sedimentology (Burgess et al., 2019). Autogenic or inherent controls are

46 those within the system, such as flow process or local structure development (e.g., Covault et
47 al., 2007; Picot et al., 2016), whilst allogenic controls are external to the sedimentary system,
48 such as sediment supply or regional tectonics (e.g., Prelat and Hodgson 2013; Soutter et al.,
49 2019). The geomorphology resulting from structural deformation influences accommodation
50 and whether a deep-marine sedimentary system is fully confined (e.g., Sinclair and Tomasso
51 2002; Marini et al, 2015, 2016a, b), partially confined, with potential for downstream bypass
52 (e.g., Deptuck et al., 2008; Casciano et al., 2019; McArthur and McCaffrey 2019), or
53 unconfined, with unrestricted run-out of flows (e.g., Normark, 1978; Normark et al., 1983;
54 Clift et al., 2002; Jegou et al., 2008; Savoye et al., 2009). Submarine lobe deposits
55 demonstrate a range of dimensions and stacking patterns depending on this confinement, with
56 lateral offset stacking demonstrated in unconfined settings (e.g., Prelat et al., 2010; Brunt et
57 al., 2013; Spychala et al., 2017; Maselli et al., 2019), or more complex stacking patterns in
58 fully- to partially-confined settings (e.g., Haughton, 2000; Etienne et al., 2012; Spychala et
59 al., 2015; Tinterri and Tagliaferri, 2015). Regardless of setting, lobe complexes typically do
60 not grow beyond tens of metres in thickness before shutdown or lobe avulsion (Prelat et al.,
61 2010; Macdonald et al., 2011; Straub and Pyles, 2012). In highly- to fully-confined settings,
62 lateral migration may not be possible, leading to the formation of ponded, sheet-like
63 turbidites (Sinclair and Tomasso 2002; Marini et al, 2015, 2016a, b). In such settings, the co-
64 deposition of most or all of the finer grained suspended load in association with coarser
65 sediment fractions commonly leads to the formation of muddy caps to successive sandy event
66 beds (Patacci et al., 2015; Marini et al. 2016b; Dorrell et al., 2018).

67 When confinement is tectonically controlled, it is thought that interaction of
68 successive turbidity currents with evolving seafloor structures may result in the development
69 of more complex deposits in terms of thickness and co-deposition of different grain size
70 classes (e.g., Sinclair and Tomasso, 2002; Brunt et al., 2004, Noda, 2018; Butler, 2019;

71 Soutter et al., 2019). However, the sparsity of both outcrop and subsurface studies of such
72 confined systems limits our understanding of the interplay between sedimentary and tectonic
73 processes and the effects upon the resulting stratigraphic architecture. Here, we address this
74 knowledge gap by documenting both outcropping and subsurface systems from trench-slope
75 basins of the Hikurangi subduction margin, on and offshore of the North Island of New
76 Zealand (Fig. 1). Only by integrating high resolution, bed-scale sedimentological outcrop
77 studies with large-scale 3D seismic analysis from the same area can we get a full
78 understanding of the stratigraphic architecture, basin structure and system evolution. In this
79 fold and thrust belt setting, Neogene lobe complexes adjacent to growth structures are
80 anomalously thick (>200 m) and form highly amalgamated, sand-rich sequences within
81 dominantly silt to mudstone prone basins. Specific objectives are to: 1) integrate studies of
82 high-resolution outcrop and large-scale seismic architectures to interpret the geological
83 processes (sedimentary and structural) and depositional setting capable of perpetuating bed
84 amalgamation during the accumulation of thick, sand-rich lobe complexes deposited in
85 tectonically active settings; 2) consider the variable influence of auto- and allogenic controls
86 on the development of deep-marine lobe complexes in areas of active seafloor deformation;
87 3) develop a depositional model for the interaction of deep-marine sedimentation and active
88 structure growth on submarine slopes; 4) assess the implications for the timing and
89 distribution of syn-kinematic lobe complex development in deep-marine fold and thrust belts.

90 Development of such understanding is important as submarine lobes may act as carbon
91 sinks (e.g., Rabouille et al., 2019), host hydrocarbon reservoirs (e.g., Prather, 2003; Saller et
92 al., 2008), and reservoirs for low carbon initiatives, such as carbon capture and storage.

93 **GEOLOGICAL SETTING**

94 This work concerns the Miocene to Recent sequence of the Hikurangi subduction
95 margin (Fig. 1). Prior to the onset of Cenozoic subduction, Zealandia was largely submerged
96 (Reyners, 2013; Strogon et al., 2014), with widespread deposition of Paleogene deep-marine
97 carbonates and marls (Fig. 2; Lillie, 1953; Chanier and Ferriere, 1991). Hikurangi subduction
98 began ca. 25 Ma, associated with the convergence of the Pacific and Australian plates (Rait et
99 al., 1991; Nicol et al., 2007; Reyners, 2013). The overriding Australian Plate has undergone
100 significant internal deformation throughout the Neogene, resulting in the development of
101 dominantly ENE-WSW-trending reverse faults with subsidiary normal and strike-slip faulting
102 (Fig. 1; Chanier and Ferriere, 1991; Beanland et al., 1998; Nicol et al., 2007; Barnes et al.,
103 2010), and of NE-SW elongated fold and thrust-bounded trench-slope basins (Bailleul et al.,
104 2013; McArthur et al., 2019). Although a general migration of deformation towards the
105 trench is seen, emplacement of thrusts and folds was out of sequence (Chanier & Ferriere
106 1991; Bailleul et al. 2013).

107 Three phases of deformation have been documented during the Neogene, which can
108 be associated with the response of the overriding plate to changes in the style of subduction
109 (Fig. 2; Wells, 1989; Chanier and Ferriere, 1991; Nicol et al., 2007). These phases correspond
110 to: 1) compression, uplift and associated emplacement of thrust nappes in the latest Oligocene
111 to Early Miocene related to the onset of subduction (Chanier and Ferriere, 1991; Rait et al.,
112 1991); 2) a mixed phase of tectonic collapse-related extension and continued convergence
113 during the Middle to Late Miocene, resulting in normal faulting on the margin (Chanier et al.,
114 1999; Barnes et al., 2002; Bailleul et al., 2013); 3) resumption of margin-wide compression
115 from the latest Miocene to present. The last phase is responsible for the development of the
116 modern margin, with uplift and exhumation of the North Island Axial and Coastal Ranges,
117 the latter corresponding to the western, exhumed, inner portion of the subduction wedge (Fig.
118 3; Nicol and Beavan, 2003; Litchfield et al., 2007; Nicol et al., 2007; Bailleul et al., 2013;

119 Jiao et al., 2015). The evolution of the subduction wedge can be traced by the infill of the
120 trench-slope basins, the innermost of which have a Miocene aged fill, with progressively
121 younger sediments towards the Hikurangi Trench (Fig. 2; Lewis and Pettinga, 1993).

122 The Plio-Pleistocene history of the margin not only records significant uplift, due to
123 acceleration of subduction, but also shortening within the fold and thrust belt, as well as
124 frontal accretion at the trench (Barnes and de Lepinay, 1997; Beanland et al., 1998; Nicol et
125 al., 2002; Litchfield et al., 2007; Reyners et al., 2011; Barnes et al., 2018). Offshore, the
126 subduction wedge displays a stepped profile, with trench-slope basins evolving on the back
127 limbs of thrust-cored structural highs (Lewis and Pettinga, 1993; Barnes et al., 2010).

128 Thin-skinned deformation on the trench-facing side of the upper plate resulted in
129 dominantly deep-marine sedimentation in the trench-slope basins (Nicol et al., 2007;
130 Burgreen and Graham, 2014). The stratigraphic record is punctuated by a series of
131 unconformities and episodes of syn-sedimentary deformation, indicative of a strong tectonic
132 influence on the sedimentation (Neef, 1992; Bailleul et al., 2007, 2013; Burgreen-Chan et al.,
133 2016). The fill of the trench-slope basins includes deep-marine mudstones, siltstones,
134 turbidites, mass-transport deposits and carbonates (Fig. 2; Lee and Begg, 2002). Typically,
135 the fill of the outcropping basins consists of regularly bedded, mud-rich turbidites, as well as
136 shallow-marine fringes (Bailleul et al., 2007). Although tortuous paths of sediment transport
137 may be expected on such margins, this is not always the case, as observed here (McArthur
138 and McCaffrey, 2019; Crisostomo Figueroa et al., 2020) and other subduction margins (e.g.,
139 Cascadia [Nelson et al., 2000] or the Makran [Bourget et al., 2011]), where transverse
140 channels may bypass significant portions of the slope.

141 Specifically, we examine outcropping Lower Miocene strata of the Greenhollows
142 Formation (Fig. 2), which was estimated at 370 m thick by Neef (1992) or 600 m by Francis

143 and Johansen (2011), implying a large degree of thickness variation across the basin (Fig. 3;
144 Bailleul et al., 2007). In the study area, these syn-subduction strata outcrop within the Akitio
145 Syncline (Neef, 1992), which is bounded to the southeast by the Coastal Block and to the
146 northwest by the Pongaroa Block (Fig. 3). The western limb of this syncline is transected by
147 the N-S trending Breakdown Fault Zone (Fig. 3; Neef, 1992, Malié et al., 2017), whereas
148 further north, second order folding is expressed by the Auster and the Paripapa synclines,
149 separated by the Kawakawa Anticline (Fig. 3; Lee and Begg, 2002). The outcrops correspond
150 to the preserved portion of the Miocene Akitio trench-slope basin (Bailleul et al., 2007). The
151 multi-phase tectonic history not only controlled the sediment distribution within that area, but
152 also the successive migration and deformation of the basin edges, as well as subsequent
153 erosion (Bailleul et al., 2013). To the southeast of Pongaroa, the Greenhollows Formation
154 shows extensional structures associated with the Middle to Late Miocene episode of
155 deformation (Malié et al., 2017). These normal faults and small-scale grabens are overprinted
156 by thrusts and reverse faults resulting from the third phase of deformation, with a shortening
157 also responsible for the larger scale folding and uplift of the entire area (Bailleul et al., 2013).

158 In the subsurface, we examine the structure and fill of the Porangahau Trough and
159 adjacent structural ridges (Fig. 1). Based upon regional seismic mapping and ties to nearby
160 wells this basin fill is interpreted as Late Miocene to Recent in age (McArthur and
161 McCaffrey, 2019). The trough is aligned NE-SW, bounded to the NW by the Madden Fault
162 and to the SE by the Porangahau Fault (Fig. 2). The structure appears simpler than the more
163 mature onshore basin, with purely convergent structures reported in this basin (Barnes et al.,
164 2010; McArthur et al., 2019), which is younger than the phase of extension reported in the
165 interior of the margin. The basin fill was dominantly sourced from the palaeo-Madden
166 Canyon (McArthur and McCaffrey, 2019) and preserves up to 2 km of sediments, with the
167 focus here on ca. 300 m of reflectors in the middle of the basin fill.

168

METHODS

169

Outcrop sedimentology

170

171

172

173

174

175

176

177

178

179

180

181

182

183

184

185

186

We examine the Lower Miocene (Burdigalian) succession of the Akitio Basin (Fig. 3), with fieldwork conducted to characterise the lithofacies, stratigraphic architecture and depositional environments. Field mapping data were recorded with a Trimble® TDC100 (Fig. 3). Sedimentary logging was conducted at bed scale (1:50), across seven sections, totalling 542 m (Fig. 3). Three hundred and fifty-five palaeocurrent indicators were measured from three-dimensional ripples, flute casts, tool marks and primary current lineations. A lithofacies scheme was developed and lithofacies associations were used to group similar packages of sediments, metres to hundreds of metres thick. These data were supplemented by information from micropalaeontological analysis conducted by GNS Science New Zealand to define the age of deposition and depositional environment. Samples were taken from hemipelagic mudstone to avoid dating potentially reworked microfossils. Photographs of key outcrops were taken to document the stratigraphic architecture, assisted by drone reconnaissance using a DJI™ Mavic Pro. Digitally mapped lithofacies associations were integrated with aerial photographs (courtesy of Land Information New Zealand – LINZ), existing biostratigraphic information (The Fossil Record Electronic Database [<https://fred.org.nz/>]) and petrophysical data (see below) in order to correlate and determine the stratigraphic distribution of the depositional elements.

187

Outcrop gamma-ray spectrometry

188

189

190

191

Rock surfaces were cleaned with a rock pick, pry-bar, drilling hammer and brush to remove the first 5 cm of the weathering surface. Natural gamma radiation was measured using a Gr320 enviSPEC Portable Gamma-ray Spectrometer. The Gr320 records total counts and ppm of ⁴⁰K, ²³⁸U and ²³²Th during a pre-selected counting period of 120 seconds. The

192 same machine and technique as described by Braaksma et al. (2003) was used. During
193 measurement the detector was placed perpendicular to the bedding. Measurements were made
194 every 50 cm where possible to relate the petrophysical properties to geological parameters.
195 Due to the edge effect and the 84 cm sampling radius of the sensor, efforts were made to
196 measure within beds >84 cm thick. However, where not possible, beds <84 cm thick were
197 measured; these data may have interference from adjacent beds. In combination with the
198 sedimentology and palaeontology, the data can help to refine interpretations of the
199 depositional system (Slatt et al., 1992).

200 *Seismic data*

201 Depth-converted 3D seismic data acquired at broadband frequency in 2017 by
202 WesternGeco was used to assess the structure and stratigraphic architecture of offshore
203 trench-slope basins. Data were interpreted using Schlumberger's Petrel© E&P and Eliis'
204 Paleoscan™ software platforms; full stack data are displayed in SEG positive, such that a
205 downward decrease in acoustic impedance is represented by a trough and a downward
206 increase is represented by a peak. This study focuses on the Madden Channel area, located in
207 the western part of the 3D seismic survey (Fig. 1). Major faults and structures were
208 interpreted and regional surfaces were extrapolated from the 3D survey; two well ties enabled
209 the base Pliocene reflector to be picked by correlation through 2D surveys (Fig. 1 and 2).
210 Attribute mapping was used to create root-mean-square (RMS) of amplitude horizon maps
211 through the interval of interest.

212 **FACIES AND ASSOCIATIONS**

213 *Lithofacies*

214 Detailed sedimentary logging permitted seven lithofacies to be identified based upon
215 their composition, primary grain size, bed thickness and lateral continuity (Table 1). These
216 comprise tabular, medium to thick-bedded, fine-grained sandstones (LF1); lenticular, thick-
217 bedded, fine-grained sandstones (LF2); discontinuous thin- to medium-bedded sandstones
218 and siltstones (LF3); tabular thin- to medium-bedded, fine-grained sandstones, siltstones and
219 mudstones (LF4); alternations of fine-grained argillaceous sandstones and mud-clast
220 conglomerates (LF5); beds of coarse bioclastic material (LF6); and massive marine
221 mudstones (LF7).

222 *Lithofacies associations*

223 Associations of the lithofacies are grouped into packages of related strata, to identify
224 stratigraphic architecture and associated depositional environments. Below, the three
225 principal lithofacies associations (lobe axis, lobe fringe and mass-transport deposits) are
226 described, then interpreted in sequence.

227 **Lithofacies Association 1 (LA1) – Lobe axis. ---**

228 Observations: Lithofacies Association 1 (LA1; Fig. 4) is characterised by tabular,
229 thick-bedded, typically amalgamated and often-dewatered sandstones (LF1), with rare
230 turbidite fines (LF4), often interbedded with discontinuous thin-beds (LF3), lenticular, thick-
231 bedded sandstones (LF2) and very rarely argillaceous sandstones and genetically-related
232 conglomerates (LF5). Occasionally beds of coarse bioclastic material (LF6) are also seen,
233 typically underlying thicker sandstones (LF1); most beds show disseminated plant debris.
234 This association is often amalgamated into packages tens to hundreds of metres thick (Fig. 5),
235 of vertically stacked, high net to gross (N:G) deposits. Sandstones often show internal scours,
236 grain-size breaks and mud-clasts aligned along horizons, indicating amalgamation of beds
237 (Fig. 4C). Bioturbation is typically restricted to the rare mud-caps and includes large burrows

238 such as *Ophiomorpha* sp. and *Thalassinoides* sp. Sole marks and other traction structures are
239 rare but generally show a south-easterly palaeocurrent direction, with a mean of 135°. In the
240 Akitio Basin this association is seen on the preserved SE edge of the basin, where this
241 association can be mapped over 12 km² (Fig. 3). Logged sections L1 and L2 provide two
242 transects through this association, converging towards the top of these logs in the Owahanga
243 Gorge area (Figs. 3 and 5). The lower logged sections total to 98 m thickness (Logs 1-2 in
244 Fig. 5), but only cover the well-exposed interval. The overlying section is poorly-exposed and
245 occurs along a the Owahanga River, with sporadically outcropping sandstones totalling a
246 further 75 m of strata. A final well-exposed section covers 22 m of strata (Log 3 in Fig. 5),
247 such that LA1 is 195 m in thickness in this locality. Although LA1 appears as a relatively
248 homogenous, sand-rich association, the gamma ray response demonstrates some distinct
249 trends, with peaks and troughs that may be used to aid lateral correlations with the coeval
250 LA2 (Fig. 5).

251 Interpretations: Supported by the observations and interpretation of the laterally
252 adjacent LA2 (see below), these laterally extensive, tabular, often amalgamated sandstone
253 dominated deposits are interpreted as a ca. 200 m thick, vertically superimposed stack of
254 submarine lobe complex axes (*sensu* Prelat et al., 2009). The apparent absence of lateral
255 offset stacking indicates that successive lobe depocentres were fixed in the same locality.
256 Although aggradational lobe complexes have been recognised elsewhere (e.g., Prather et al.,
257 1998; Sychala et al., 2017), they develop thicknesses that are substantially less than those
258 demonstrated here, before avulsion or abandonment of the system terminates turbidite
259 deposition (der Merwe et al., 2014). Palaeocurrent directions to the SE indicate that the flow
260 was perpendicular to the NE-SW trending basin edge (Fig. 3), which was likely less than 2
261 km away during deposition (Bailleul et al. 2013). Very thin or absent mud-caps imply
262 downstream bypass of suspended fines; rare thin-bedded turbidite intervals exhibit signs of

263 sustained, rather than waning flow. More commonly, repeated erosion of the upper surfaces
264 of turbidites resulted in the development of an amalgamated series of sandstones (Stow and
265 Johansson, 2000). However, no significant scour surfaces were seen here, nor partially
266 preserved thicker mud-caps.

267 Micropalaeontology samples from this association indicates a late Burdigalian age
268 and deposition in mid-bathyal depths (>700 m). Without sedimentological evidence of shut
269 down of the lobe system, individual lobe complexes are not immediately evident in outcrop.
270 However, in the spectral gamma ray log a series of sharp based units with repeated
271 decreasing log response permit the definition of multiple lobe complexes (Fig. 5), with the
272 maximum thickness of any individual lobe complex being 80 m (Fig. 5). Mechanisms to
273 control this anomalously thick accumulation of lobe sediments in this confined, tectonically
274 active setting are discussed below.

275 **Lithofacies Association 2 (LA2) – Lobe fringes. ---**

276 Observations: This association comprises tabular thin-bedded turbidites (LF4), with
277 sporadic thicker beds (LF1) separated by mudstones (LF7), hybrid beds (LF5) and rare
278 lenticular sandstones (LF2) (Fig. 6). As with LA1, some beds may be associated with
279 bioclastic grits (LF6) and most beds show disseminated plant debris. LA2 deposits are seen to
280 grade up from LA1 (Fig. 5) or simply from thick intervals of LF7 (Fig. 7), occurring across
281 the mapped Upper Burdigalian extent of the Akitio Basin (Fig. 3); i.e. this association is seen
282 across the remainder of the contemporary basin fill where LA1 is not present. The thickness
283 of this association is highly variable across the basin, with exposures ranging from tens to
284 hundreds of metres in thickness (Fig. 7). Overall this association is more heterolithic,
285 includes more hybrid event beds (LF5) and has a lower N:G, but exhibits less structures than
286 LA1 (Fig. 8). Unlike LA1, some intervals of hemipelagic mudstone (LF7) up to 250 cm thick

287 are present (Fig. 7). Bioturbation is common to intense across all lithofacies and as with LA1
288 includes *Ophiomorpha* sp. and *Thalassinoides* sp, but rare to abundant *Chondrites* sp.,
289 *Nerites* sp. and *Phycosiphon* sp. are also identified. Sole marks and other structures exhibit
290 mean palaeocurrent directions similar to LA1 (142°), but with a slightly wider spread (Fig. 8).
291 Where preserved, the top of this association is typically truncated by a basin-wide MTD (Fig.
292 3) (see LA3 below). Although showing a similar range of gamma ray responses to LA1
293 (typically around 20-30 counts per 120 seconds), the gamma ray character of this association
294 shows higher frequency changes in vertical log response than LA1 and distinct breaks in the
295 trend (Fig. 9).

296 Interpretations: These laterally extensive, sandstone-rich deposits are interpreted as
297 lateral lobe fringes (*sensu* Spychala et al., 2017). The decreased N:G, increased presence of
298 hybrid beds and lateral association with LA1 imply these sediments are not laterally
299 continuous, sheet-like deposits across the basin (e.g., Prather et al., 2012; Patacci et al.,
300 2015), but form the fringes to a lobe system (Prelat et al., 2009; Kane et al., 2017). Despite
301 showing mud-caps, these differ from the ponded turbidites of the underlying system in that
302 beds show slightly fewer traction structures, more variable palaeocurrent orientations,
303 interpreted to represent flow deflections and have a wider variety of bed thicknesses (Fig. 7
304 and 8; Bailleul et al., 2007). With run-out of flows towards the lobe fringes greater mudstone
305 deposition is inferred, as opposed to the bypass and potential erosion of bed tops in the axial
306 portion. The hemipelagic mudstone dominated intervals may represent periods of shutdown
307 (Fig. 7), i.e. they may separate seven different lobe complexes, which are harder to recognise
308 in the amalgamated axis (LA1), but discernible in the lobe fringe (LA2).

309 As with LA1, micropalaeontology samples from this association indicate a late
310 Burdigalian age and deposition in mid-bathyal depths (>700 m). It is clearer to divide the
311 deposits of LA2 than those of LA1 into lobe complexes. This can be done based upon their

312 sedimentology, with mudstone-dominated intervals between complexes (Fig. 7). The
313 petrophysical measurements agree with the sedimentological division into seven lobe
314 complexes, with each complex defined by peaks in the gamma ray total followed by gradual
315 reduction, allowing correlations with LA1 (Fig. 9).

316 **Lithofacies Association 3 (LA3) – Mass-transport deposits. ---**

317 Observations: This association comprises clasts of all lithofacies, ranging from pebble
318 size to tens of metres thick and tens to hundreds of metres long, forming jumbled packages,
319 metres up to ca. 100 m thick (Fig. 6C). Commonly clasts are composed of LF3-4, or blocks
320 of carbonate rocks, bioclastic sandstone (LF6) or mudstone (LF7). Rafts are generally
321 internally coherent and good quality outcrops are required to identify the often-subtle
322 juxtaposition of rafts and to observe basal shear zones or large-scale folding of rafts. The
323 matrix is composed of silty mudstone and may contain floating bioclastic debris. The matrix
324 may form from <20% to >80%, of the deposit, often grading within it. Where an obvious
325 erosion surface and truncation of underlying strata is not present, careful measurement of
326 bedding orientations between sheared zones may also help to distinguish this association
327 from in-situ deposits. A relatively thin (<5 m thick) example of this facies association is seen
328 to underlie LA1 at the base of log 1 (Fig. 5), whilst several thinner examples underlie the
329 LA2 (Fig. 7). Both LA1 and LA2 are overlain by a single event (L3 shown in Fig. 5), which
330 has a variable thickness across the basin of up to 100 m and shows an erosive base (Fig. 6).

331 Interpretations: These often seismic-scale intervals are interpreted as mass-transport
332 deposits (MTDs), remobilising sediments deposited within the basins and on their edges.
333 Bioclastic debris may have been derived from shallow-marine facies that periodically
334 developed on the basin edges (Bailleul et al., 2007). The widespread occurrence of these
335 deposits indicates that they filled or partially filled basins, as can be observed in modern

336 basins offshore New Zealand, such as the Paritu Basin (Mountjoy and Micallef, 2012). The
337 largest MTDs appear to be associated with significant changes in both accommodation and
338 subsequent basin evolution, with different facies associations seen above the major MTDs
339 compared with those beneath them (see description of Middle Miocene strata in McArthur
340 and McCaffrey, 2019), implying either the MTDs or events that triggered them were
341 responsible for such changes. The large MTD overlying the sequence shows significant
342 erosion into both LA1 and LA2 (Fig. 6). Although it is difficult to determine the amount of
343 erosion, this may be greater in the axial portion, as described in the subsurface example
344 below. Although MTDs are pervasive in New Zealand stratigraphy, we have confidence that
345 the studied interval between the documented MTDs (i.e., LA1-2) is in-situ, demonstrating dip
346 and strike consistent with the regional strata (unlike the MTDs), no signs of internal slide or
347 scour surfaces and presenting coherent stratigraphy correlatable over distances, which is not
348 possible in MTDs.

349 *Seismic facies*

350 Although detail on the sedimentary systems is gained from outcrop studies, the large-
351 scale nature of the stratal architecture is difficult to resolve. Therefore, a comparison with
352 similar systems imaged in the subsurface is appropriate to observe the preserved extent of the
353 deposits (Fig. 10) and help understand the tectono-stratigraphic evolution. Analysis of
354 seismic reflection data from the same margin allows us to examine the fill of offshore trench-
355 slope basins, in the actively developing portion of the subduction wedge (McArthur et al.,
356 2019), specifically the Porangahau Trough (Fig. 1). To aid this workflow, packages of
357 reflectors with similar characteristics are defined. Five seismofacies are interpreted based
358 upon their seismic amplitude, frequency, termination style and internal character to represent
359 background hemipelagic sedimentation (SF1); sheet-like sediments with alternating character

360 (SF2); submarine channel fills (SF3); lobe complexes (SF4); and mass-transport deposits
361 (SF5) (see Table 2 and the following text for description and interpretation).

362 *Seismic facies associations*

363 Associations of the seismofacies can be grouped into packages of related reflectors, to
364 identify stratigraphic architecture and basin setting. Below, the three principal seismofacies
365 associations (SA) are described then interpreted, being pre-lobe strata (SA1), aggradational
366 lobe complexes (SA2) and post-lobe strata (SA3). Attribute analysis was conducted to aid
367 interpretation in the interval of interest (Fig. 12; supplementary video).

368 **Seismofacies Association 1 (SA1) – Pre-lobe strata. ---**

369 Observations: Seismofacies Association 1 (SA1) is characterised by low amplitude,
370 low frequency, laterally continuous reflectors (SF1) and alternating high and low amplitude,
371 low frequency reflectors (SF2) (Fig. 10). The faulted and folded reflectors that form the
372 substrate to the trench-slope basins mostly comprise low amplitude, chaotic reflectors
373 (deformed SF1; Fig. 10). Within these reflectors, several faults and folds are imaged, with the
374 principal structures defining the edges or sills of the basins (Fig. 11). The sills are thus
375 underpinned by thrust-cored detachment folds, which at present extends NNE-SSW some ca.
376 75 km laterally along the margin. The western structure has a vertical throw of 2.5 km but is
377 complicated by several detachment horizons (Fig. 10); the eastern structure has a minimum
378 vertical throw of 3 km, however erosion of the crest of the sill is apparent (Fig. 12). A sharp
379 surface overlies and truncates these lower reflectors, above which are alternating mostly low
380 amplitude reflectors of SF2 and subordinate SF1, which are laterally continuous across
381 individual basins but onlap against the basin edges (Fig. 11A and B). No distinctive
382 geomorphological features are seen in mapped 3D surfaces within these reflectors.

383 Interpretations: A series of thrust faults and associated folds can be seen in the highly
384 deformed reflectors at depth (SF1), here interpreted to represent pre-subduction strata *sensu*
385 McArthur et al. (2019). The sharp surface overlying these reflectors is interpreted as a
386 regional unconformity, marking the onset of the effects of subduction in this area, creation of
387 individual trench-slope basins and initiation of their infill (Fig. 10). Above this surface,
388 reflectors of SF1 and SF2 are seen to pond within the basin centre and onlap the edges (e.g.,
389 Prather et al., 1998). That no sedimentary features are imaged within SA1 (i.e., channels,
390 lobes etc.) implies these represent a low energy infill. Note that the structures within the pre-
391 subduction interval penetrate and influence the geometry of this package, but not the
392 overlying reflectors, implying that deformation became focused on the basin bounding
393 structures during deposition of SA2 and stopped thereafter. The basin bounding sill is formed
394 by a thrust-cored detachment fold. Given that it affects the seafloor today, the expression of
395 the sill during deposition cannot be precisely constrained, although it is clear that it was
396 forming a topographic barrier on the seafloor at the time of deposition and causing growth
397 strata in the adjacent basin.

398 **Seismofacies Association 2 (SA2) – Aggradational lobe complexes. ---**

399 Observations: Overlying the laterally continuous reflectors are a series of reflectors
400 that are discontinuous at basin scale, mostly represented by SF4 within the core of the basin,
401 fringed by SF1, whilst SF3 and SF5 are present in the up-dip portion (Fig. 11). SF3 is
402 represented by lenticular, concave-up units that are kilometres wide and hundreds of metres
403 thick, seen to truncate underlying reflectors and that are filled with relatively heterogeneous
404 reflectors (Fig. 11). A prominent expression of SF3 is seen to cut the up-dip structure (Fig.
405 11G and H). SF4 is represented by semi-continuous, mounded, convex-up, mostly high
406 amplitude reflectors, which are seen to downlap at their fringes, forming a radial pattern
407 approximately 8 km in diameter in front of the downstream sill as illustrated in Figure 11H.

408 Mapping of horizons and RMS amplitude extractions of horizons through the interval
409 dominated by SF4 demonstrate a complex array of high amplitude reflectors immediately
410 down-dip of the structure separating the Porangahau Trough from the basin immediately
411 upslope (Fig. 12A). These reflectors can be separated into at least five separate packages,
412 each tens of metres thick (varying laterally from ca. 20 to 70 m thick) and generally stacking
413 vertically to over 300 m thick (Fig. 11). Within the high amplitude reflectors, isolated lenses,
414 tens of metres wide and up to kilometres in length, extend out from the upstream (i.e., NW)
415 structure across the high amplitude area (Fig. 12). Subsequent downstream basins only show
416 low amplitude reflectors over this interval (Fig. 12). However, at least three such occurrences
417 of similar successions of reflector packages are seen in other basins of the subduction wedge
418 (Fig. 12A).

419 Interpretations: The discontinuous reflector packages above SA1 characterise a
420 variety of depositional styles. The lenticular and erosional SF3 is interpreted to represent the
421 fill of submarine channels (e.g., Mayall and Stewart, 2000). For example, a major channel
422 complex is interpreted to cross-cut the up-dip structure and acted as the primary sediment
423 conduit feeding the basin (Fig. 11; 12A); this being the ancient expression of the Madden
424 Channel (Fig. 1). The first discontinuous deposits in the basin are clearly an MTD (Fig. 12B),
425 however no significant megaclasts are resolved, thereby suggesting this MTD didn't form
426 any significant seafloor topography.

427 The discontinuous, radial, downlapping reflectors of SF4 are interpreted as submarine
428 lobe complexes (*sensu* Booth et al., 2003). At least four lobe complexes can be defined at the
429 base of the intra-basinal palaeo-slope (Fig. 11, 12). These sediments were fed through the up-
430 dip channel and stack vertically behind the downstream sill (Fig. 11; Fig. 12C), giving a
431 sustained, aggradational stacking pattern, as the confinement did not allow for significant
432 lateral offset stacking (*sensu* Prelat et al., 2009). This confinement and lack of lateral

433 migration may explain why the feeder channel fill is approximately the same width as the
434 lobe complexes. The radial pattern implies that along slope currents were not influential in
435 the basin at this time, as they later became (Bailey et al., 2020). The finger-like features seen
436 on RMS extractions of the lobes are interpreted as distributary channels (e.g., Fig. 11G; 12D;
437 Maier et al., 2020), which can be seen approaching the sill. Restriction of the high amplitude
438 responses to areas behind the sill implies that coarse-grained sediments were trapped behind
439 this growth structure (Fig. 12E). However, attribute extractions show an evolution of the
440 interaction with the sill during deposition of the lobes, with the first three complexes being
441 entirely trapped behind the sill (Fig. 12C, D and E), but eventually displaying a low
442 amplitude shadow across the sill and into the downstream accommodation, which could
443 imply bypass of fines (Fig. 12F). Ultimately, erosion of the sill's crest is seen (Fig. 12F) and
444 higher amplitudes begin to develop in the basin downstream, which may have occurred due
445 to overspill and bypass of coarser material.

446 **Seismofacies Association 3 (SA3) – Post-lobe strata. ---**

447 Observations: The radial reflectors of SA2 are terminated by a chaotic interval of SF5
448 tens of metres thick (Fig. 11). The deposits of SF5 are seen to have both been sourced
449 through the feeder conduit and also to have been shed from the flanks of the basin bounding
450 structures (Fig. 12G). Those fed through the up-dip conduit appear to truncate the proximal
451 deposits of SF4, whilst those from the local structures simply overly SF4. Above this,
452 alternating reflectors of SF1, 3 and 5 combine to fill the basin to the seafloor.

453 Interpretations: Ultimately the whole system was significantly modified after the
454 emplacement of a major MTD over the lobe complexes, which shows great erosion into the
455 axial portion of the lobes, either directly preceding or contemporaneous to the MTD
456 emplacement (Fig. 12G). This MTD was sourced remotely and fed through the same channel

457 system that supplied the lobe complexes. Emplacement of additional smaller, lateral MTDs is
458 thought to relate to local collapse of the up-dip structure and may indicate a renewed phase of
459 deformation.

460 Lobe deposition is inferred to have been terminated either as a result of MTD
461 emplacement, which potentially damned the upstream channel (c.f., McArthur and
462 McCaffrey, 2019), or by a change in the deformation style, due to the associated diversion of
463 the sediment dispersal pathway elsewhere (c.f., McArthur et al., 2019). Alternatively, the
464 sediment supply could simply have been switched off. Recurrences of channel complexes
465 (SF3) above lobe systems implies that basin filling and development of bypass conduits
466 connecting to downstream basins is a common phenomenon (Fig. 11), as is seen in the
467 outcropping succession (McArthur and McCaffrey, 2019), with relatively unconfined MTDs,
468 hemipelagites and contourites providing the overburden (Bailey et al., 2020).

469 **INTEGRATION AND INTERPRETATION OF TECTONO-STRATIGRAPHIC** 470 **ARCHITECTURE**

471 Distinctive patterns of sedimentation can be observed in detail at outcrop, at larger
472 scale in seismic data and integrated to leverage a clearer understanding of the tectono-
473 stratigraphic evolution of confined intra-slope basins. At outcrop scale, the petrophysical data
474 enable a correlation of the lobe axis and fringe deposits to be made (Fig. 9), which implies
475 that a greater thickness of fringe deposits is preserved within the outcropping basin than at
476 the axis. A similar thickness discrepancy is seen from axis to fringe deposits in the subsurface
477 example, with the lobe axis being incised and eroded (Fig. 11 and 12). This may be a result of
478 erosion over the position of the lobe axis by the overlying MTD or due to periods of
479 sustained bypass of fines during deposition of coarser-grained axial deposits. A combination

480 is likely, with lateral correlation of the more bypass prone axial complexes to thicker
481 intervals of fringe deposits (Fig. 9).

482 In both outcrop and subsurface examples, lobe complexes of similar dimensions
483 (hundreds of metres thick [minimum 10 m, maximum 70 m] by approximately 15 km²; Figs.
484 3 and 12), overlie older, ponded sediments, indicating that the basins had formed and seafloor
485 relief had been generated by structural activity, both within the basins and on their edges
486 (Fig. 3; 11). The deposition of the lobes suggests that the deformation became focused on the
487 basin bounding structures, with intra-basinal structures no longer exerting an influence on the
488 seafloor. Even if it is difficult to establish at outcrop, this is clearly seen in the subsurface,
489 where reflectors of SA1 were deformed and vary in thickness adjacent to structures, whilst
490 those of SA2 are not deformed (Fig. 10). Although both outcrop and subsurface examples
491 shown in this study overlie muddy MTDs they are not significantly thick, being <5 m at
492 outcrop and ca. 20 m thick in the subsurface, nor do they include megaclasts; therefore, large-
493 scale ponding on top of these MTDs is not envisaged.

494 At the time of lobe inception, the basin-bounding structures were still exerting an
495 influence on the seafloor, as illustrated by the trapping of the coarse sediment within these
496 depocentres (Fig. 3; 12). However, both at outcrop and in the subsurface, the clastic sediment
497 dispersal system did not terminate with the sandstone component of the lobes (e.g.,
498 Boulesteix et al., 2019), and not even within the same basin as where the lobes were
499 deposited (Fig. 12). The lobes in outcrop do not show a frontal fringe, but show palaeoflow
500 towards the basin sill (Fig. 8). In the subsurface a continuation of lower amplitude reflectors
501 across and over the downstream sill is seen in amplitude mapping, implying the bypass of
502 fines beyond the high amplitude lobe axis (Fig. 12A and F). Therefore, although the coarse-
503 grained component was being trapped in the proximal basins, flow stripping at the sill is
504 inferred to have occurred, with coarser-grained sediment fractions being trapped in the

505 upstream basin and with fines predominantly being carried in suspension into the adjacent
506 downslope basin (e.g., Sinclair and Tomasso, 2002). This phenomenon has been illustrated in
507 laboratory and numerical modelling of the interaction of turbidity currents with static
508 structures (Brunt et al., 2004; Lamb et al., 2004, 2006; Nasr-Azadani et al., 2013); however,
509 these simulations cannot directly model the dynamic evolution of deformation, sedimentation
510 and compaction over geological timescales.

511 In both the documented outcrop and subsurface examples, the lobe complexes are
512 seen to stack aggradationally, producing amalgamated lobe complexes hundreds of metres
513 thick; far in excess of the thicknesses typically documented in unconfined settings (e.g., Fig.
514 13; Table 3; Prelat et al., 2009; Macdonald et al., 2011; Straub and Pyles, 2012; Cullis et al.,
515 2019). More typically, lobe complexes are seen to be separated by thinner bedded, muddier
516 sediment, either representing a shutdown or an avulsion of the sedimentary system (Prelat et
517 al., 2009). A lateral and vertical transition to finer grained, thinner-bedded strata (LA2) is
518 seen at outcrop (Fig. 9), whilst lower amplitude reflectors (SF1) are seen across the remainder
519 of the basin imaged in the subsurface (Fig. 12A). That these coarse sediments are isolated
520 within a dominantly fine-grained system implies that regional changes in sediment supply
521 along the margin was unlikely responsible for the variation in sediment type (Fig. 2), if such
522 a scenario existed a similar caliber of deposits would be expected all along the margin (Fig.
523 12A). Although similar thicknesses have been documented for alternations of channel
524 complexes, lobe complexes and MTDs in the northern portion of the Hikurangi Margin
525 (Burgreen and Graham, 2014), those lobe complexes are offset along the trench-slope basin
526 axis rather than aggradationally stacked, consequently with a lower N:G than described in the
527 axial deposits here.

528 Taking the thickness of the biostratigraphically constrained outcropping lobes at 200
529 m over an interval of at maximum 2.8 Ma (NZ Altonian stage 18.7 – 15.9 Ma) would give an

552 erosion of the sill, which would rapidly lead to the development of a spill conduit and
553 wholesale downstream bypass (e.g., Casciano et al., 2019).

554 2) Net sediment aggradation rate < sill uplift rate

555 Growth of bounding structures at rates greater than sediment supply and burial would
556 result in a return to ponded conditions, potentially developing a sheet-like fill across the basin
557 (e.g., Prather et al., 2012; Patacci et al., 2015). This scenario is contrary to the observed
558 variation in sediment distribution and lack of thick mud-caps (Dorrell et al., 2018).

559 3) Net sediment aggradation rate \approx sill uplift rate

560 In order to sustain the effectively fixed confinement condition required to develop the
561 aggradational lobe complexes described here, a balance between growth of the basin
562 bounding structures and net sedimentation rate is required. Under the scenario in which
563 sedimentation rates and structure growth rates are set independently this condition would
564 seem unlikely to arise frequently; yet here we document multiple instances of aggradationally
565 stacked lobe complexes developed upstream of sills across space and time. Although the
566 development of stacked lobe complexes tens of metres thick trapped in local accommodation
567 has been documented (e.g., Tinterri and Muzzi Magalhaes, 2011; Tinterri and Tagliaferri,
568 2015), these local depocentres are typically rapidly filled by the sediment input, resulting in a
569 migration of the depocentre.

570 Structure growth alone cannot account for the observed stratal thickness, with rates of
571 fault movement in the study area being insufficient to maintain accommodation with high
572 rates of sediment influx (Barnes and Nicol, 2004). Studies have shown that growth of faults
573 and fault related-folds can be intrinsically linked to the sedimentary fill and loading of
574 accommodation (e.g., Noda, 2018; Butler, 2019; Serck and Braathen, 2019). To account for

575 the common development of fixed confinement conditions for extended periods we suggest
576 that a feedback mechanism of sediment – structure interaction may operate (Fig. 14).
577 Initially, sediment ponding in the basin centre was onlapping the basin edges, whilst syn-
578 sedimentary deformation was related to intra-basinal structures (Fig. 14A). This model
579 proposes that sediment loading within the basin eventually results in focusing of stress on the
580 basin bounding faults, with abandonment of the previously active intra-basinal structures as
581 they are buried (Fig. 14B). Continued trapping of coarse sediment behind the growth
582 structure results in sustained sediment loading, coupled with growth of the sill (Fig. 14C-D),
583 permitting the development of vertically stacked lobe complexes hundreds of metres thick.
584 The isostatic loading and focusing of stress on the basin bounding structures may also help to
585 perpetuate tectonic loading in front of the growth structures, further driving generation of
586 accommodation space (Fig. 14D).

587 Ultimately, external forcing (e.g., sediment re-routing, switch-off of sediment supply,
588 progressive outboard migration of deformation, wholesale changes in the style of
589 deformation, or the emplacement of basin-wide MTDs) disrupts the balanced interaction of
590 sedimentation and structuration, resulting in a change in sedimentary style (Fig. 14E). Similar
591 models of sediment load-driven subsidence have been proposed for salt domains (Vendeville,
592 2005), but hitherto have not been explicitly interpreted to operate in fold and thrust belts.
593 Stress modelling of the margin evolution and / or advanced forward modelling of basin
594 structure and fill will help constrain this evolution, but is beyond the scope of this study.

595 These concepts of sedimentation modulating structure growth and hence accommodation
596 raise the potential for similar deposits in other fold and thrust belts. For example Cascadia
597 (Nelson et al., 2000), the deep-water portion of the Makran (Bourget et al., 2011) and
598 offshore Sabah (Jackson et al., 2009).

599 *Allogenic vs autogenic influences on confined lobe complex stacking patterns*

600 An interplay of auto- and allogenic factors is inferred to contribute to the evolution of
601 the aggradational lobe complexes by generating a sill whose relative elevation with respect to
602 the aggrading sediment surface was relatively invariant (Fig. 15). Protracted and repeated
603 flow stripping over this sill, with preferential bypass of fines, i.e. an autogenic control,
604 resulted in the development of aggradationally stacked lobe complexes hundreds of metres
605 thick (Fig. 15A-C). As with lobe complexes observed by Burgreen and Graham (2014) in the
606 northern portion of the Hikurangi Margin, these lobes appear to form very thick,
607 amalgamated complexes, implying that they were likely deposited in tortuous corridors in
608 this convergent setting. However, the interpretation of Burgreen and Graham (2014) that the
609 lobes were migrating along the axis of the trench-slope basin is not applicable in either of the
610 examples documented here. Aggradational lobe complexes described elsewhere cannot
611 compare to the thicknesses observed here (Table 3; Fig. 13). However, the spatial extent of
612 these confined lobe complexes is limited compared to the scale of other documented lobe
613 complexes (Prelat et al., 2010), which may be self-regulating, scaling with size of the
614 generated accommodation. Variability in factors such as turbidity flow thickness, turbidity
615 current frequency and incremental compaction-related subsidence may have influenced
616 individual bed development but are unlikely to have affected the first-order pattern of
617 stratigraphic architecture, which is seen repeatedly in the fill of trench-slope basins on this
618 margin.

619 Overspill of fines into downstream basins may result in the development of thick
620 intervals of turbidite silt- and mudstone there (Fig. 15C). Recognition of this process in the
621 subsurface may be difficult (Volvoikar et al., 2020). Therefore, it may be challenging to
622 distinguish thick intervals of rapidly accumulated turbidite fines from those of slowly

623 accumulated pelagic or hemipelagic sediments, and thus to establish accurate sedimentation
624 rates in trench-slope basin fills (e.g., Boulesteix et al., 2019).

625 In both examples shown here, external forcing is seen to modify the system to the
626 degree that sediment pathways were fundamentally altered (Fig. 15D). Similar effects have
627 been documented in other confined deep-marine settings (e.g., Haughton, 2000; Soutter et al.,
628 2019). The MTD emplacement across the basin may have been related to a wider
629 modification of the margin structure and could also have blocked or diverted the sediment
630 supply or otherwise destabilised the balance of sedimentation and deformation (e.g., Bull et
631 al., 2020). Alteration of the regional stress field (unbalancing the feedback mechanism
632 invoked here or causing structuration that diverted flow pathways) or a significant decrease
633 or increase of the sediment supply could also disrupt the maintenance of a partial-ponding
634 condition, leading to changes in the sedimentary system.

635 *Implications for active margin resource distribution*

636 The aggradational lobe complexes documented here represent the cleanest and
637 thickest development of potentially reservoir-grade sediments within the trench-slope basins,
638 be that for conventional hydrocarbons, as aquifers, or as sites for carbon sequestration.
639 Although unpublished, a similar model of sediment-structure interaction has been invoked to
640 explain the presence of ca. 200 m of stacked sandstones in the Troika Field, Gulf of Mexico.
641 This is also within a system that is overall relatively mud-rich, albeit in a different tectonic
642 setting (Horine et al., 2000). Therefore, our model may help explain the presence of
643 anomalously thick deep-marine sandstones in subsurface examples where deposition
644 occurred in a confined setting (Kirkova-Pourciau and Hill, 2004).

645 In particular, subsequently inverted basins may develop suitable structural closures
646 within which the lobes may be located. Although the lobe complexes are dominantly

647 aggradational, a minor degree of compensational stacking (Fig. 10) implies they are not
648 entirely as simple as purely vertically stacked reservoir and consideration of variable
649 reservoir properties across different lobe complexes may be anticipated in a vertical section.
650 Abandoned structures underlying the basins may act as fluid pathways to charge intra-basinal
651 lobe complexes (Fig. 10).

652 Identification of these units in the subsurface may prove difficult, particularly after
653 deformation responsible for trap formation. Therefore, a schematic wireline log signature
654 generated from the outcropping systems may aid exploration in such settings (Fig. 16).
655 Bypass-dominated fine-grained intervals, occurring in discontinuous lenses (Fig. 4A), are not
656 laterally extensive and would not act as barriers to fluid flow. Conversely, the mudstones of
657 the lobe fringe, or those accumulating in downstream basins, would likely be laterally
658 continuous, presenting baffles or barriers to flow.

659 CONCLUSIONS

660 The relationship between deep-marine sedimentation and deformation has been
661 investigated from trench-slope basin fill and structure from the Hikurangi subduction margin,
662 New Zealand. Information from outcropping and subsurface basins on the same margin has
663 been integrated to describe sandstone-rich submarine lobe complexes, aggrading and
664 amalgamated into packages hundreds of meters thick. When possible, the integration of the
665 detailed sedimentology afforded by outcrops with the seismic scale system architecture yields
666 novel insights to the evolution of sedimentary systems and their interaction with growth
667 structures. Here, outcrop studies and seismic data analysis indicate that flow stripping
668 occurred as turbidity currents encountered seafloor structures, resulting in the accumulation
669 of sand-rich deposits behind thrust-cored sills whose thickness implies that a partial ponding
670 condition was maintained for extended periods. Simple scenarios of passive basin infill

671 cannot account for the continued accumulation of these deposits, which reach 300 m in
672 thickness, nor can scenarios with no links between the tectonic rejuvenation of confinement
673 and ongoing sedimentation. Accordingly, a depositional model for sedimentary modulation of
674 tectonic structure growth is proposed in which:

- 675 • An influx of sediment into confined basins drives isostatic loading and
676 suppresses intrabasinal structure growth, focusing stress onto basin bounding
677 faults.
- 678 • Activity on basin bounding faults maintains the development of
679 accommodation and relatively fixed, but partial confinement enables the
680 repeated deposition of thick-bedded, clean, amalgamated sandstones, forming
681 aggradational lobe complexes hundreds of metres thick, as finer-grained
682 sediment fractions are stripped and bypassed to deeper basins. This constitutes
683 an autogenic control on the development of lobe complexes.
- 684 • Eventually allogenic forcing (e.g., regional mass-transport deposit
685 emplacement, upstream modification of feeder pathways, significant changes
686 in the sediment flux and/or the rates of deformation) alters the sedimentary
687 system, such that turbidite lobes no longer form at the same locality.

688 Therefore, sediment flux and loading are inferred to interact with the tectonism,
689 creating a feedback loop, with implications for the tectono-stratigraphic evolution of deep-
690 marine fold and thrust belts. This coupling of sedimentation and deformation may have
691 resulted in the accumulation of thick syn-kinematic turbidite lobe complexes in other
692 confined basins during times of optimally balanced structural evolution and sediment flux.
693 Although amalgamated lobe complexes may be hundreds of meters thick, their areal extent
694 may genetically tie to the wavelength of deformation, hence limiting their areal distribution.

695 This study effectively permits the inference of a range of conditions under which partial
696 confinement can be maintained. A linkage between sedimentation and deformation is
697 proposed, with sediment input rates high enough to prevent development of full ponding and
698 allowing partial bypass, but not so high as to cause erosion on the sill and complete bypass.
699 Understanding the bounding conditions that lead to such accumulations may help define
700 deep-marine sediment sinks and enhance resource exploration in deep-marine fold and thrust
701 belts.

702 **ACKNOWLEDGEMENTS**

703 This research was funded by a JIP between Chevron, Equinor, OMV and
704 Schlumberger. WesternGeco Multiclient are thanked for permission to publish seismic data.
705 Hugh Morgans of GNS and the information contained in the New Zealand Fossil Record File
706 are acknowledged for foraminifera biostratigraphy. Land owners are kindly thanked for
707 access to the study area. Many thanks to field assistants Vanisha Pullan and Nick Zajac; Alan
708 Clare, Petter Bjørgen and Frank Chanier for thoughtful insights; David Francis of Geological
709 Research for introduction to the field area and Cécile Robin for helping JuB measure
710 sections. We thank Associated Editor Amy Weislogel and reviewers Katherine Maier and
711 Nora Nieminski for their helpful and constructive reviews.

712 **REFERENCES**

- 713 Bailey, W.E., McArthur, A.D., and McCaffrey, W.D., 2020. Distribution of contourite drifts
714 on convergent margins: examples from the Hikurangi subduction margin of NZ.
715 *Sedimentology*, pp. 55. doi:10.1111/SED.12779
- 716 Bailleul, J., Chanier, F., Ferrière, J., Robin, C., Nicol, A., Mahieux, G., Gorini, C., and Caron,
717 V., 2013, Neogene evolution of lower trench-slope basins and wedge development in the

- 718 central hikurangi subduction margin, new zealand: *Tectonophysics*, v. 591, p. 152–174,
719 doi: 10.1016/j.tecto.2013.01.003.
- 720 Bailleul, J., Robin, C., Chanier, F., Guillocheau, F., Field, B., and Ferriere, J., 2007, Turbidite
721 Systems in the Inner Forearc Domain of the Hikurangi Convergent Margin (New
722 Zealand): New Constraints on the Development of Trench-Slope Basins: *Journal of*
723 *Sedimentary Research*, v. 77, p. 263–283, doi: 10.2110/jsr.2007.028.
- 724 Barnes, P.M., and de Lepinay, B.M., 1997, Rates and mechanics of rapid frontal accretion
725 along the very obliquely convergent southern Hikurangi margin , New Zealand: *Journal*
726 *of Geophysical Research*, v. 102, p. 24,931-24,952, doi: 10.1029/97JB01384.
- 727 Barnes, P.M., and Nicol, A., 2004, Formation of an active thrust triangle zone associated with
728 structural inversion in a subduction setting, eastern New Zealand: *Tectonics*, v. 23.
- 729 Barnes, P.M., Nicol, A., and Harrison, T., 2002, Late Cenozoic evolution and earthquake
730 potential of an active listric thrust complex above the Hikurangi subduction zone, New
731 Zealand: *Geological Society of America Bulletin*, v. 114, p. 1379–1405.
- 732 Barnes, P.M., Lamarche, G., Bialas, J., Henrys, S., Pecher, I., Netzeband, G.L., Greinert, J.,
733 Mountjoy, J.J., Pedley, K., and Crutchley, G., 2010, Tectonic and geological framework
734 for gas hydrates and cold seeps on the Hikurangi subduction margin, New Zealand:
735 *Marine Geology*, v. 272, p. 26–48, doi: 10.1016/j.margeo.2009.03.012.
- 736 Barnes, P.M., Ghisetti, F.C., Ellis, S., and Morgan, J.K., 2018, The role of protothrusts in
737 frontal accretion and accommodation of plate convergence, Hikurangi subduction
738 margin, New Zealand: *Geosphere*, v. 14, p. 440–468, doi: 10.1130/GES01552.1.
- 739 Beanland, S., Melhuish, A., Nicol, A., and Ravens, J., 1998, Structure and deformational
740 history of the inner forearc region, Hikurangi subduction margin, New Zealand: *New*

- 741 Zealand Journal of Geology and Geophysics, v. 41, p. 325–342, doi:
742 10.1080/00288306.1998.9514814.
- 743 Booth, J.R., Dean, M.C., DuVernay, A.E., and Styzen, M.J., 2003, Paleo-bathymetric
744 controls on the stratigraphic architecture and reservoir development of confined fans in
745 the Auger Basin: central Gulf of Mexico slope: *Marine and Petroleum Geology*, v. 20, p.
746 563–586, doi: 10.1016/j.marpetgeo.2003.03.008.
- 747 Boulesteix, K., Poyatos-Moré, M., Flint, S.S., Taylor, K.G., Hodgson, D.M. and Hasiotis,
748 S.T., 2019, Transport and deposition of mud in deep-water environments: Processes and
749 stratigraphic implications: *Sedimentology*, v. 66, p.2894-2925.
- 750 Bourget, J., Zaragosi, S., Mulder, T., Schneider, J.L., Garlan, T., Van Toer, A., Mas, V., and
751 Ellouz-Zimmermann, N., 2010, Hyperpycnal-fed turbidite lobe architecture and recent
752 sedimentary processes: A case study from the Al Batha turbidite system, Oman margin:
753 *Sedimentary Geology*, v. 229, p. 144-159.
- 754 Bourget, J., Zaragosi, S., Ellouz-Zimmermann, N., Mouchot, N., Garlan, T., Schneider, J.L.,
755 Lanfumeu, V. and Lallemand, S., 2011, Turbidite system architecture and sedimentary
756 processes along topographically complex slopes: the Makran convergent
757 margin: *Sedimentology*, v. 58, p.376-406.
- 758 Braaksma, H., Kenter, J.A.M., Proust, J.N., Z, Dijkmans, V., Van Hoek, T, Mahieux, G. and
759 Drijkoningen, G.G., 2003, Controls on acoustic properties of Upper Jurassic siliciclastic
760 rocks (Boulonnais, northern France): *Geophysics*, v. 68, p. 58-69.
- 761 Brunt, R.L., McAffrey, W.D., and Kneller, B.C., 2004, Experimental modeling of the spatial
762 distribution of grain size developed in a fill-and-spill mini-basin setting: *Journal of*
763 *Sedimentary Research*, v. 74, p. 438–446.

- 764 Brunt, R.L., Hodgson, D.M., Flint, S.S., Pringle, J.K., Di Celma, C., Prélat, A., and Grecula,
765 M., 2013, Confined to unconfined: Anatomy of a base of slope succession, Karoo Basin,
766 South Africa: *Marine and Petroleum Geology*, v. 41, doi:
767 10.1016/j.marpetgeo.2012.02.007.
- 768 Burgess, P. M., Masiero, I., Toby, S. C. and Duller, R. A., 2019,. A Big Fan of Signals?
769 Exploring Autogenic and Allogenic Process and Product In a Numerical Stratigraphic
770 Forward Model of Submarine-Fan Development: *Journal of Sedimentary Research* v.
771 89, p. 1-12.
- 772 Burgreen, B., and Graham, S., 2014, Evolution of a deep-water lobe system in the Neogene
773 trench-slope setting of the East Coast Basin, New Zealand: Lobe stratigraphy and
774 architecture in a weakly confined basin configuration: *Marine and Petroleum Geology*,
775 v. 54, p. 1–22, doi: 10.1016/j.marpetgeo.2014.02.011.
- 776 Burgreen-Chan, B., Meisling, K.E., and Graham, S., 2016, Basin and petroleum system
777 modelling of the East Coast Basin, New Zealand: a test of overpressure scenarios in a
778 convergent margin: *Basin Research*, v. 28, p. 536–567, doi: 10.1111/bre.12121.
- 779 Bull, S., Browne, G.H., Arnot, M.J. and Strachan, L.J., 2020, Influence of mass transport
780 deposit (MTD) surface topography on deep-water deposition: an example from a
781 predominantly fine-grained continental margin, New Zealand. Geological Society,
782 London, Special Publications, v. 500, pp. 25.
- 783 Butler, R.W.H., 2019, Syn-kinematic strata influence the structural evolution of emergent
784 fold-thrust belts: Geological Society, London, Special Publications, v. 490, p. SP490--
785 2019.
- 786 Casciano, C. I., Patacci, M., Longhitano, S. G., Tropeano, M., McCaffrey, W. D. and Di

- 787 Celma, C., 2019, Multi-scale analysis of a migrating submarine channel system in a
788 tectonically-confined basin: The Miocene Gorgoglione Flysch Formation, southern
789 Italy: *Sedimentology* v. 66, p. 205-240.
- 790 Chanier, F., and Ferriere, J., 1991, From a passive to an active margin; tectonic and
791 sedimentary processes linked to the birth of an accretionary prism (Hikurangi Margin,
792 New Zealand): *Bulletin de la Société géologique de France*, v. 162, p. 649–660.
- 793 Chanier, F., Ferrière, J., and Angelier, J., 1999, Extensional deformation across an active
794 margin, relations with subsidence, uplift, and rotations: The Hikurangi subduction, New
795 Zealand: *Tectonics*, v. 18, p. 862–876, doi: 10.1029/1999TC900028.
- 796 Clift, P., Gaedicke, C., Edwards, R., Lee, J. Il, Hildebrand, P., Amjad, S., White, R.S., and
797 Schlüter, H.-U., 2002, The stratigraphic evolution of the Indus Fan and the history of
798 sedimentation in the Arabian Sea: *Marine Geophysical Researches*, v. 23, p. 223–245.
- 799 Cohen, K.M., Finney, S.C., Gibbard, P.L., and Fan, J.-X., 2013, The ICS international
800 chronostratigraphic chart: *Episodes*, v. 36, p. 199–204.
- 801 Covault, J.A., Normark, W.R., Romans, B.W., and Graham, S.A., 2007, Highstand fans in the
802 California borderland: The overlooked deep-water depositional systems: *Geology*, v.35,
803 p. 783–786.
- 804 Crisostomo Figueroa, A., McArthur, A.D., Dorrel, R., Amy, L., and McCaffrey, W.D., 2020,
805 A new modelling approach to sediment bypass prediction applied to the East Coast
806 Basin, New Zealand: *Geological Society of America Bulletin*, pp. 15,
807 <https://doi.org/10.1130/B35687.1>
- 808 Cullis, S., Patacci, M., Colombera, L., Bührig, L. and McCaffrey, W.D., 2019, A database
809 solution for the quantitative characterisation and comparison of deep-marine siliciclastic

- 810 depositional systems: *Marine and Petroleum Geology*, v. 102, p.321-339.
- 811 Dennielou, B., Droz, L., Babonneau, N., Jacq, C., Bonnel, C., Picot, M., Le Saout, M., Saout,
812 Y., Bez, M., Savoye, B. and Olu, K., 2017, Morphology, structure, composition and
813 build-up processes of the active channel-mouth lobe complex of the Congo deep-sea fan
814 with inputs from remotely operated underwater vehicle (ROV) multibeam and video
815 surveys: *Deep Sea Research Part II: Topical Studies in Oceanography*, v. 142, p.25-49.
- 816 Deptuck, M.E., Piper, D.J.W., Savoye, B., and Gervais, A., 2008, Dimensions and
817 architecture of late Pleistocene submarine lobes off the northern margin of East Corsica:
818 *Sedimentology*, v. 55, p. 869–898.
- 819 Dorrell, R. M., Patacci, M., and McCaffrey, W. D., 2018, Inflation of Ponded, Particulate
820 Laden Density Currents: *Journal of Sedimentary Research*, v.88, p.1276-1282.
- 821 Etienne, S., Mulder, T., Bez, M., Desaubliaux, G., Kwasniewski, A., Parize, O., Dujoncquoy,
822 E., and Salles, T., 2012, Multiple scale characterization of sand-rich distal lobe deposit
823 variability: examples from the Annot Sandstones Formation, Eocene--Oligocene, SE
824 France: *Sedimentary Geology*, v. 273, p. 1–18.
- 825 Figueiredo, J.J.P., Hodgson, D.M., Flint, S.S., and Kavanagh, J.P., 2010, Depositional
826 environments and sequence stratigraphy of an exhumed Permian mudstone-dominated
827 submarine slope succession, Karoo Basin, South Africa: *Journal of Sedimentary
828 Research*, v. 80, p. 97-118.
- 829 Figueiredo, J.J.P., Hodgson, D.M., Flint, S.S., and Kavanagh, J.P., 2013, Architecture of a
830 channel complex formed and filled during long-term degradation and entrenchment on
831 the upper submarine slope, Unit F, Fort Brown Fm., SW Karoo Basin, South Africa:
832 *Marine And Petroleum Geology*, v. 41, p. 104-116.

- 833 Flint S.S., Hodgson, D.M., Sprague, A.R., Brunt, R.L., van der Merwe, W.C., Figueiredo
834 J.J.P., Prelat A., Box D., Di Celma C.N., and Kavanagh J.P., 2011, Depositional
835 architecture and sequence stratigraphy of the Karoo basin floor to shelf edge succession,
836 Laingsburg depocentre, South Africa: *Marine And Petroleum Geology*, v.28, p. 658-674.
- 837 Flood, R.D., Manley, P.L., Kowsmann, R.O., Appi, C.J., and Pirmez, C., 1991, Seismic
838 facies and late Quaternary growth of Amazon submarine fan, in Weimer, P., and Link,
839 M.H., eds., *Seismic facies and sedimentary processes of submarine fans and turbidite
840 systems.*, New York, NY, United States, Springer-Verlag, p. 415-433.
- 841 Francis, D.A., and Johansen, A., 2011, *Geology of the Kawakawa Structure: Ministry of
842 Economic Development New Zealand, Petroleum Report Series PR4482*, 48 p.
- 843 Grecula, M., Flint, S.S., Wickens, H. d.V., and Johnson, S.D., 2003 Upward-thickening
844 patterns and lateral continuity of Permian sand-rich turbidite channel fills, Laingsburg
845 Karoo, South Africa: *Sedimentology*, v. 50, p. 831-853.
- 846 Grundvag, S.-A., Johannessen, E.P., Helland-Hansen, W., Plink-Bjoerklund, P., 2014,
847 Depositional architecture and evolution of progradationally stacked lobe complexes in
848 the Eocene Central Basin of Spitsbergen: *Sedimentology*, v.61, p. 535-569.
- 849 Houghton, P.D.W., 2000, Evolving turbidite systems on a deforming basin floor, Tabernas,
850 SE Spain: *Sedimentology*, v. 47, p. 497–518.
- 851 Houghton, P.D., Barker, S.P. and McCaffrey, W.D., 2003, ‘Linked’debrites in sand-rich
852 turbidite systems—origin and significance: *Sedimentology*, v. 50, p.459-482.
- 853 Heron, D.W. (custodian), 2014, *Geological map of New Zealand 1:250,000. Lower Hutt,*
854 *NZ: GNS Science. GNS Science geological map 1. 1 CD.*

- 855 Hofstra, M., Hodgson, D.M., Peakall, J., and Flint, S.S., 2015, Giant scour-fills in ancient
856 channel-lobe transition zones: Formative processes and depositional architecture:
857 Sedimentary Geology, v. 329, p. 98-114.
- 858 Horine, R.L., Mills, W.H., Sturrock, V.J., and Anthony, M., 2000, Structural controls on
859 sedimentation and hydrocarbon charge in the Troika Field—deepwater Gulf of Mexico
860 (abstract): American Association of Petroleum Geologists, 2000 Annual Meeting,
861 Abstract Volume, p. A69.
- 862 Jackson, C.A.L., Zakaria, A.A., Johnson, H.D., Tongkul, F., and Crevello, P.D., 2009,
863 Sedimentology, stratigraphic occurrence and origin of linked debrites in the West
864 Crocker Formation (Oligo-Miocene), Sabah, NW Borneo: Marine and Petroleum
865 Geology, v. 26, p.1957-1973.
- 866 Jegou, I., Savoye, B., Pirmez, C., and Droz, L., 2008, Channel-mouth lobe complex of the
867 recent Amazon Fan: the missing piece: Marine Geology, v. 252, p. 62–77.
- 868 Jiao, R., Seward, D., Little, T.A., and Kohn, B.P., 2015, Unroofing of fore-arc ranges along
869 the Hikurangi Margin, New Zealand: Constraints from low-temperature
870 thermochronology: Tectonophysics, v. 656, p.39-51.
- 871 Joseph, P., Babonneau, N., Bourgeois, A., Cotteret, G., Eschard, R., Garin, B., Gomes De
872 Souza, O., Granjeon, D., Guillocheau, F., Lerat, O., and Quemener, J.M., 2000: The
873 Annot Sandstone outcrops (French Alps): architecture description as input for
874 quantification and 3D reservoir modeling, *in* Weimer, P., ed., Deep-Water Reservoirs of
875 the World: Gulf Coast Section SEPM Foundation 20th Annual Research Conference,
876 SEPM Special Publication, V. 28, p. 422-449.
- 877 Jobe, Z.R., Sylvester, Z., Howes, N., Pirmez, C., Parker, A., Cantelli, A., Smith, R.,

- 878 Wolinsky, M.A., O'Byrne, C., Slowey, N., and Prather, B., 2017, High-resolution,
879 millennial-scale patterns of bed compensation on a sand-rich intraslope submarine fan,
880 western Niger Delta slope: Geological Society of America Bulletin, v. 129, p. 23-37.
- 881 Jobe, Z.R., Howes, N., Romans, B.W., Covault, J.A., 2018, Volume and recurrence of
882 submarine-fan-building turbidity currents: Depositional Record, v. 4, p. 160-176.
- 883 Kane, I.A., McCaffrey, W.D., and Martinsen, O.J., 2009, Allogenic vs. autogenic controls on
884 megaflute formation: Journal of Sedimentary Research, v. 79, p.643-651.
- 885 Kane, I.A., Pontén, A.S.M., Vangdal, B., Eggenhuisen, J.T., Hodgson, D.M., and Spychala,
886 Y.T., 2017, The stratigraphic record and processes of turbidity current transformation
887 across deep-marine lobes: Sedimentology, v. 64, p. 1236-1273.
- 888 Kirkova-Pourciau, J.T., and Hill, W.A., 2004, Seismic Facies Mapping on the Major
889 Reservoir Producer (S10) in the Troika Field: Gulf Coast Association of Geological
890 Societies Transactions, v. 54, p. 305-312.
- 891 Kneller, B. and McCaffrey, W., 1999, Depositional effects of flow nonuniformity and
892 stratification within turbidity currents approaching a bounding slope; deflection,
893 reflection, and facies variation: Journal of Sedimentary Research, v. 69, p.980-991.
- 894 Iorio, M., Liddicoat, J.C., Budillon, F., Tiano, P., Incoronato, A., Coe, R.S., and Marsella, E.,
895 2009, Paleomagnetic secular variation time constraints on late Neogen geological events
896 in slope sediment from the eastern Tyrrhenian Sea, *in* Kneller, B.C., Martinsen, O.J., and
897 McCaffrey, W.D., eds. External Controls on Deep-Water Depositional Systems: Society
898 for Sedimentary Geology, Special Publication v. 92, p. 233-243.
- 899 Lamb, M.P., Hickson, T., Marr, J.G., Sheets, B., Paola, C., and Parker, G., 2004, Surging
900 versus continuous turbidity currents: flow dynamics and deposits in an experimental

- 901 intraslope minibasin: *Journal of Sedimentary Research*, v. 74, p. 148–155.
- 902 Lamb, M.P., Toniolo, H., and Parker, G., 2006, Trapping of sustained turbidity currents by
903 intraslope minibasins: *Sedimentology*, v. 53, p. 147–160.
- 904 Lee, J.M. and Begg, J.G., 2002, *Geology of the Wairarapa area: Institute of Geological &
905 Nuclear Sciences 1:250,000 geological map 11. 1 sheet + 66 pages. Institute of
906 Geological and Nuclear Sciences Ltd, Lower Hutt, New Zealand.*
- 907 Lericolais, G., Bourget, J., Popescu, I., Jermannaud, P., Mulder, T., Jorry, S., and Panin, N.,
908 2013, Late Quaternary deep-sea sedimentation in the western Black Sea: New insights
909 from recent coring and seismic data in the deep basin: *Global and Planetary Change*, v.
910 103, p. 232-247.
- 911 Lewis, K.B., and Pettinga, J.R., 1993, The emerging, imbricate frontal wedge of the
912 Hikurangi margin: *Sedimentary basins of the world*, v. 2, p. 225–250.
- 913 Lillie, A.R., 1953, *The geology of the Dannevirke Subdivision: New Zealand Geological
914 Survey bulletin*, v. 46, 156 p.
- 915 Litchfield, N., Ellis, S., Berryman, K., and Nicol, A., 2007, Insights into subduction-related
916 uplift along the Hikurangi Margin, New Zealand, using numerical modeling: *Journal of
917 Geophysical Research: Earth Surface*, v. 112, p. 1–17, doi: 10.1029/2006JF000535.
- 918 Liu, Q., Kneller, B.C., Fallgatter, C., and Buso, V.V., 2018, Quantitative comparisons of
919 depositional architectures of unconfined and confined turbidite sheet systems:
920 *Sedimentary Geology*, v. 376, p. 72-89.
- 921 Macdonald, H.A., Peakall, J., Wignall, P.B., and Best, J., 2011, Sedimentation in deep-sea
922 lobe-elements: implications for the origin of thickening-upward sequences: *Journal of*

- 923 the Geological Society, v. 168, p. 319–332.
- 924 Maier, K.L., Paull, C.K., Caress, D.W., Anderson, K., Nieminski, N.M., Lundsten, E., Erwin,
925 B.E., Gwiazda, R., and Fildani, A., 2020, Submarine-fan development revealed by
926 integrated high-resolution datasets from La Jolla Fan, offshore California, USA: Journal
927 of Sedimentary Research, v. 90, p.468-479.
- 928 Malié, P., Bailleul, J., Chanier, F., Toullec, R., Mahieux, G., Caron, V., Field, B., Mählmann,
929 R.F., and Potel, S., 2017, Spatial distribution and tectonic framework of fossil tubular
930 concretions as onshore analogues of cold seep plumbing systems, North Island of New
931 Zealand. Bulletin de la Société géologique de France, v. 188, pp. 25.
- 932 Marini, M., Milli, S., Ravnas, R., and Moscatelli, M., 2015, A comparative study of confined
933 vs. semi-confined turbidite lobes from the Lower Messinian Laga Basin (Central
934 Apennines, Italy): Implications for assessment of reservoir architecture: Marine and
935 Petroleum Geology, v.63, p.142-165.
- 936 Marini, M., Patacci, M., Felletti, F., and McCaffrey, W.D., 2016a, Fill to spill stratigraphic
937 evolution of a confined turbidite mini-basin succession, and its likely well bore
938 expression: The Castagnola Fm, NW Italy: Marine and Petroleum Geology, v. 69, p. 94–
939 111.
- 940 Marini, M., Felletti, F., Milli, S., and Patacci, M., 2016b, The thick-bedded tail of turbidite
941 thickness distribution as a proxy for flow confinement: Examples from tertiary basins of
942 central and northern Apennines (Italy): Sedimentary Geology, v.341, p.96-118.
- 943 Maselli, V., Kneller, B., Taiwo, O.L., and Iacopini, D., 2019, Sea floor bedforms and their
944 influence on slope accommodation: Marine and Petroleum Geology, v. 102, p. 625–637.
- 945 Mayall, M., and Stewart, I., 2000, The Architecture of Turbidite Slope Channels, *in* Deep-

- 946 Water Reservoirs of the World: 20th Annual, Society of Economic Paleontologists and
947 Mineralogists, v. Deep-Water, p. 578–586, doi: 10.5724/gcs.00.15.0578.
- 948 Mayall, M., Lonergan, L., Bowman, A., James, S., Mills, K., Primmer, T., Pope, D., Rogers,
949 L. and Skeene, R., 2010, The response of turbidite slope channels to growth-induced
950 seabed topography: AAPG Bulletin, v.94, p.1011–1030.
- 951 McArthur, A.D., and McCaffrey, W.D., 2019, Sedimentary architecture of detached deep-
952 marine canyons: Examples from the East Coast Basin of New Zealand: *Sedimentology*,
953 v. 66, p. 1067–1101.
- 954 McArthur, A.D., Claussmann, B., Bailleul, J., McCaffrey, W., and Clare, A., 2019, Variation
955 in syn-subduction sedimentation patterns from inner to outer portions of deep-water fold
956 and thrust belts: examples from the Hikurangi subduction margin of New Zealand:
957 Geological Society, London, Special Publications, v. 490, p. SP490--2018.
- 958 der Merwe, W.C., Hodgson, D.M., Brunt, R.L., and Flint, S.S., 2014, Depositional
959 architecture of sand-attached and sand-detached channel-lobe transition zones on an
960 exhumed stepped slope mapped over a 2500 km² area: *Geosphere*, v. 10, p. 1076–1093.
- 961 Mountjoy, J.J., and Micallef, A., 2012, Polyphase emplacement of a 30 km³ blocky debris
962 avalanche and its role in slope-gully development, *in* *Submarine Mass Movements and
963 Their Consequences*, Springer, p. 213–222.
- 964 Nasr-Azadani, M.M., Hall, B., and Meiburg, E., 2013, Polydisperse turbidity currents
965 propagating over complex topography: comparison of experimental and depth-resolved
966 simulation results: *Computers & Geosciences*, v. 53, p. 141–153.
- 967 Neef, G., 1992, Turbidite deposition in five miocene, bathyal formations along an active plate
968 margin, North Island, New Zealand: with notes on styles of deposition at the margins of

- 969 east coast bathyal basins: *Sedimentary Geology*, v. 78, p. 111–136, doi: 10.1016/0037-
970 0738(92)90116-9.
- 971 Nelson, C.H., Goldfinger, C., Johnson, J.E. and Dunhill, G., 2000, Variation of modern
972 turbidite systems along the subduction zone margin of Cascadia Basin and implications
973 for turbidite reservoir beds, *in* Weimer, P., ed., *Deep-Water Reservoirs of the World:*
974 *20th Annual Research Conference, Gulf Coast Section Society of Economic*
975 *Paleontologists and Mineralogists*, p. 714 – 738.
- 976 Nicol, A., and Beavan, J., 2003, Shortening of an overriding plate and its implications for slip
977 on a subduction thrust, central Hikurangi Margin, New Zealand: *Tectonics*, v. 22.
- 978 Nicol, A., and Wallace, L.M., 2007, Temporal stability of deformation rates: Comparison of
979 geological and geodetic observations, Hikurangi subduction margin, New Zealand:
980 *Earth and Planetary Science Letters*, v. 258, p. 397–413, doi:
981 10.1016/j.epsl.2007.03.039.
- 982 Nicol, A., VanDissen, R., Vella, P., Alloway, B., and Melhuish, A., 2002, Growth of
983 contractional structures during the last 10 m.y. at the southern end of the emergent
984 Hikurangi forearc basin, New Zealand: *New Zealand Journal of Geology and*
985 *Geophysics*, v. 45, p. 365–385, doi: 10.1080/00288306.2002.9514979.
- 986 Nicol, A., Mazengarb, C., Chanier, F., Rait, G., Uruski, C., and Wallace, L., 2007, Tectonic
987 evolution of the active Hikurangi subduction margin, New Zealand, since the Oligocene:
988 *Tectonics*, v. 26, p. 1–24, doi: 10.1029/2006TC002090.
- 989 Noda, A., 2018, Forearc basin stratigraphy and interactions with accretionary wedge growth
990 according to the critical taper concept: *Tectonics*, v. 37, p. 965–988.
- 991 Normark, W.R., 1978, Fan Valleys, channels, and depositional lobes on modern submarine

- 992 fans; characters for recognition of sandy turbidite environments: AAPG Bulletin , v. 62,
993 p. 912–931.
- 994 Normark, W.R., Piper, D.J.W. and Hess, G.R., 1979, Distributary channels, sand lobes, and
995 mesotopography of Navy submarine fan, California Borderland, with applications to
996 ancient fan sediments: Sedimentology, v. 26, p.749-774.
- 997 Normark, W.R., Piper, D.J.W., and Stow, D.A. V, 1983, Quaternary development of
998 channels, levees, and lobes on middle Laurentian Fan: AAPG Bulletin, v. 67, p. 1400–
999 1409.
- 1000 Ortiz-Karpf, A., Hodgson, D.M. and McCaffrey, W.D., 2015, The role of mass-transport
1001 complexes in controlling channel avulsion and the subsequent sediment dispersal
1002 patterns on an active margin: the Magdalena Fan, offshore Colombia: Marine and
1003 Petroleum Geology, v.64, p.58-75.
- 1004 Patacci, M., Houghton, P.D.W., and Mccaffrey, W.D., 2015, Flow behavior of ponded
1005 turbidity currents: Journal of Sedimentary Research, v. 85, p. 885–902.
- 1006 Picot, M., Droz, L., Marsset, T., Dennielou, B., and Bez, M., 2016, Controls on turbidite
1007 sedimentation: insights from a quantitative approach of submarine channel and lobe
1008 architecture (Late Quaternary Congo Fan): Marine and Petroleum Geology, v. 72, p.
1009 423–446.
- 1010 Piper, D.J.W., and Normark, W.R., 2001, Sandy fans; from Amazon to Hueneme and
1011 beyond: AAPG Bulletin, v.85, p. 1407-1438.
- 1012 Pirmez, C., Beaubouef, R.T., Friedmann, S.J., and Mohrig, D.C., 2000, Equilibrium Profile
1013 and Baselevel in Submarine Channels: Examples from Late Pleistocene Systems and
1014 Implications for the Architecture of Deepwater Reservoirs, *in* Weimer, P., ed., Deep-

- 1015 Water Reservoirs of the World: 20th Annual Research Conference, Gulf Coast Section
1016 Society of Economic Paleontologists and Mineralogists, p. 782-805.
- 1017 Popescu, I., Lericolais, G., Panin, N., Wong, H.K., and Droz, L., 2001, Late Quaternary
1018 channel avulsions on the Danube deep-sea fan, Black Sea: *Marine Geology*, v. 179, p.
1019 25-37.
- 1020 Posamentier, H.W. and Kolla, V., 2003, Seismic geomorphology and stratigraphy of
1021 depositional deepwater deposits: *Journal of Sedimentary Research*, v.73, p.367–388.
- 1022 Postma, G., and Kleverlaan, K., 2018, Supercritical flows and their control on the architecture
1023 and facies of small-radius sand-rich fan lobes: *Sedimentary Geology*, v. 364, p. 53-70.
- 1024 Prather, B.E., 2003, Controls on reservoir distribution, architecture and stratigraphic trapping
1025 in slope settings: *Marine and Petroleum Geology*, v. 20, p. 529–545.
- 1026 Prather, B.E., Booth, J.R., Steffens, G.S., and Craig, P.A., 1998, Classification, lithologic
1027 calibration, and stratigraphic succession of seismic facies of intraslope basins, deep-
1028 water Gulf of Mexico: *AAPG bulletin*, v. 82, p. 701–728.
- 1029 Prather, B.E., Pirmez, C., and Winker, C.D., 2012, Stratigraphy of linked intraslope basins:
1030 Brazos-Trinity system western Gulf of Mexico: Application of the Principles of Seismic
1031 Geomorphology to Continental-Slope and Base-of-Slope Systems: Case Studies from
1032 Seafloor and Near-Seafloor Analogues: *SEPM, Special Publication*, v. 99, p. 83–110.
- 1033 Prelat, A., and Hodgson, D.M., 2013, The full range of turbidite bed thickness patterns in
1034 submarine lobes: controls and implications: *Geological Society of London, Journal*, v.
1035 170, p. 209–214.
- 1036 Prelat, A., Hodgson, D.M., and Flint, S.S., 2009, Evolution, architecture and hierarchy of

- 1037 distributary deep-water deposits: a high-resolution outcrop investigation from the
1038 Permian Karoo Basin, South Africa: *Sedimentology*, v. 56, p. 2132–2154, doi:
1039 10.1111/j.1365-3091.2009.01073.x.
- 1040 Prelat, A., Covault, J.A., Hodgson, D.M., Fildani, A., and Flint, S.S., 2010, Intrinsic controls
1041 on the range of volumes, morphologies, and dimensions of submarine lobes:
1042 *Sedimentary Geology*, v. 232, p. 66–76.
- 1043 Pringle, J.K., Brunt R.L., Hodgson, D.M., and Flint, S.S., 2010, Capturing stratigraphic and
1044 sedimentological complexity from submarine channel complex outcrops to digital 3D
1045 models, Karoo Basin, South Africa: *Petroleum Geoscience*, v. 16, p. 307-330.
- 1046 Pyles, D.R., Fleming, A.E.P., and Anderson, D.S., 2019, Hierarchical Organization and
1047 Spatial Variations of Lobes in Distributive Submarine Fans: Outcrop Study of the Point
1048 Loma Formation, California, USA, *in* Marsaglia, K.M., Schwalbach, J.R., and Behl,
1049 R.J., eds., *From the Mountains to the Abyss: The California Borderland as an Archive of*
1050 *Southern California Geologic Evolution*. SEPM Special Publication, v. 110, p. 135-157.
- 1051 Rabouille, C., Dennielou, B., Baudin, F., Raimonet, M., Droz, L., Khripounoff, A., Martinez,
1052 P., Mejanelle, L., Michalopoulos, P., Pastor, L., and Pruski, A., 2019, Carbon and silica
1053 megasink in deep-sea sediments of the Congo terminal lobes: *Quaternary Science*
1054 *Reviews*, v. 222, p.105854.
- 1055 Raine, J.I., Beu, A.G., Boyes, A.F., Campbell, H., Cooper, R.A., Crampton, J.S., Crundwell,
1056 M.P., Hollis, C.J., and Morgans, H.E.G., 2015, Revised calibration of the New Zealand
1057 Geological Timescale: NTGT2015/1: GNS Science Lower Hutt.
- 1058 Rait, G., Chanier, F., and Waters, D.W., 1991, Landward- and seaward-directed thrusting
1059 accompanying the onset of subduction beneath New Zealand: *Geology*, v. 19, p. 230–

- 1060 233, doi: 10.1130/0091-7613(1991)019<0230:LASDTA>2.3.CO;2.
- 1061 Reyners, M., 2013, The central role of the Hikurangi Plateau in the Cenozoic tectonics of
1062 New Zealand and the Southwest Pacific: *Earth and Planetary Science Letters*, v. 361, p.
1063 460–468, doi: 10.1016/j.epsl.2012.11.010.
- 1064 Reyners, M., Eberhart-Phillips, D., and Bannister, S., 2011, Tracking repeated subduction of
1065 the Hikurangi Plateau beneath New Zealand: *Earth and Planetary Science Letters*, v.
1066 311, p. 165–171, doi: 10.1016/j.epsl.2011.09.011.
- 1067 Saller, A., Werner, K., Sugiaman, F., Cebastian, A., May, R., Glenn, D., and Barker, C.,
1068 2008, Characteristics of Pleistocene deep-water fan lobes and their application to an
1069 upper Miocene reservoir model, offshore East Kalimantan, Indonesia: *AAPG Bulletin*,
1070 v. 92, p. 919–949, doi: 10.1306/03310807110.
- 1071 Savoye, B., Babonneau, N., Dennielou, B., and Bez, M., 2009, Geological overview of the
1072 Angola-Congo margin, the Congo deep-sea fan and its submarine valleys, *in* *Deep Sea*
1073 *Research Part II: Topical studies in Oceanography*, v. 56, p. 2169–2182.
- 1074 Sclater, J.G., and Christie, P.A.F., 1980, Continental stretching: An explanation of the post-
1075 Mid-Cretaceous subsidence of the central North Sea Basin: *Journal of Geophysical*
1076 *Research: Solid Earth*, v. 85, p. 3711–3739.
- 1077 Serck, S.C., and Braathen, A., 2019, Extensional fault and fold growth: Impact on
1078 accommodation evolution and sedimentary infill: *Basin Research*, v. 31, p. 967–990.
- 1079 Sinclair, H.D., and Tomasso, M., 2002, Depositional evolution of confined turbidite basins:
1080 *Journal of Sedimentary Research*, v. 72, p. 451–456.
- 1081 Sixsmith, P.J., Flint, S.S., Wickens, H. d.V., and Johnson, S.D., 2004, Anatomy and

- 1082 stratigraphic development of a basin floor turbidite system in the Laingsburg Formation,
1083 Main Karoo Basin, South Africa: *Journal of Sedimentary Research*, v. 74, p. 239-254.
- 1084 Slatt, R.M., Jordan, D.W., D'Agostino, A., and Gillespie, R.H., 1992, Outcrop gamma-ray
1085 logging to improve understanding of subsurface well log correlations, *in*: Hurst, A.,
1086 Griffiths, C.M., Worthington, P.F. (Eds.), *Geological Applications of Wireline Logs II*.
1087 Geological Society, London, Special Publications. v. 65, p. 3–19.
- 1088 Soutter, E.L., Kane, I.A., Fuhrmann, A., Cumberpatch, Z.A., and Huuse, M., 2019, The
1089 stratigraphic evolution of onlap in siliciclastic deep-water systems: Autogenic
1090 modulation of allogenic signals: *Journal of Sedimentary Research*, v. 89, p. 890–917.
- 1091 Spychala, Y.T., Hodgson, D.M., Flint, S.S., and Mountney, N.P., 2015, Constraining the
1092 sedimentology and stratigraphy of submarine intraslope lobe deposits using exhumed
1093 examples from the Karoo Basin, South Africa: *Sedimentary Geology*, v. 322, doi:
1094 10.1016/j.sedgeo.2015.03.013.
- 1095 Spychala, Y.T., Hodgson, D.M., Prélat, A., Kane, I.A., Flint, S.S., and Mountney, N.P., 2017,
1096 Frontal and lateral submarine lobe fringes: comparing sedimentary facies, architecture
1097 and flow processes: *Journal of Sedimentary Research*, v. 87, p. 75–96.
- 1098 Stevenson, C.J., Jackson, C.A.L., Hodgson, D.M., Hubbard, S.M. and Eggenhuisen, J.T.,
1099 2015, Deep-water sediment bypass: *Journal of Sedimentary Research*, v. 85, p.1058-
1100 1081.
- 1101 Stow, D.A. V, and Johansson, M., 2000, Deep-water massive sands: nature, origin and
1102 hydrocarbon implications: *Marine and Petroleum Geology*, v. 17, p. 145–174.
- 1103 Straub, K.M., and Pyles, D.R., 2012, Quantifying the hierarchical organization of
1104 compensation in submarine fans using surface statistics: *Journal of Sedimentary*

- 1105 Research, v. 82, p. 889–898.
- 1106 Strogon, D.P., Bland, K.J., Nicol, A., and King, P.R., 2014, Paleogeography of the Taranaki
1107 Basin region during the latest Eocene–Early Miocene and implications for the “total
1108 drowning” of Zealandia: *New Zealand Journal of Geology and Geophysics*, v. 57, p.
1109 110–127, doi: 10.1080/00288306.2014.901231.
- 1110 Tinterri, R., and Muzzi Magalhaes, P., 2011, Synsedimentary structural control on foredeep
1111 turbidites: An example from Miocene Marnoso-arenacea Formation, Northern
1112 Apennines, Italy: *Marine and Petroleum Geology*, v. 28, p. 629–657, doi:
1113 10.1016/j.marpetgeo.2010.07.007.
- 1114 Tinterri, R., and Tagliaferri, A., 2015, The syntectonic evolution of foredeep turbidites
1115 related to basin segmentation: Facies response to the increase in tectonic confinement
1116 (Marnoso-arenacea Formation, Miocene, Northern Apennines, Italy): *Marine and
1117 Petroleum Geology*, v. 67, p. 81–110.
- 1118 Tinterri, R., and Piazza, A., 2019, Turbidites facies response to the morphological
1119 confinement of a foredeep (Cervarola Sandstones Formation, Miocene, northern
1120 Apennines, Italy): *Sedimentology*, v. 66, p. 636–674.
- 1121 Van Lente, B., 2004, Chemostratigraphic trends and provenance of the Permian Tanqua and
1122 Laingsburg depocentres, southwestern Karoo basin, South Africa (Doctoral dissertation,
1123 Stellenbosch: University of Stellenbosch). pp. 339.
- 1124 Vendeville, B.C., 2005, Salt tectonics driven by sediment progradation: Part I—Mechanics
1125 and kinematics: *AAPG bulletin*, v. 89, p. 1071–1079.
- 1126 Vinnels, J.S., Butler, R.W.H., McCaffrey, W.D. and Paton, D.A., 2010, Depositional
1127 processes across the Sinu accretionary prism, offshore Colombia: *Marine and Petroleum*

1128 Geology, v.27, p.794–809.

1129 Volvoikar, S., Mazumdar, A., Peketi, A., Dewangan, P., Sawant, B., Manaskanya, A.,

1130 Goswami, H., Das, D. and Pujari, S., 2020, Contrasting sulfidization in the turbidite and

1131 hemipelagic sediments of Bengal Fan: Marine and Petroleum Geology, v. 118, 104408.

1132 Wells, P., 1989, Burial history of Late Neogene sedimentary basins on part of the New

1133 Zealand convergent plate margin: Basin Research, v. 2, p. 145–160, doi: 10.1111/j.1365-

1134 2117.1989.tb00032.x.

1135 Yang, S.-Y., and Kim, J.W., 2014, Pliocene basin-floor fan sedimentation in the Bay of

1136 Bengal (offshore northwest Myanmar): Marine And Petroleum Geology, v. 49, p. 45-58.

1137 Zhang, J.J., Wu, S.H., Fan, T.E., Fan, H.J., Jiang, L., Chen, C., Wu, Q.Y., and Lin, P., 2016,

1138 Research on the architecture of submarine-fan lobes in the Niger Delta Basin, offshore

1139 West Africa: Journal of Palaeogeography, v. 5, p. 185-204.

1140 FIGURE CAPTIONS

1141 Fig. 1. A) Geological map (Heron, 2014) and 400 m grid resolution hillshade bathymetry

1142 map (courtesy of NIWA) of the southern portion of the Hikurangi subduction margin.

1143 Seismic study focused on area around the MC - Madden Channel; PT - Porangahau Trough;

1144 and PR - Porangahau Ridge. B) Schematic cross-section of the Hikurangi subduction

1145 complex, after Nicol et al. (2007).

1146

1147 Fig. 2. Schematic chronostratigraphic chart for the southern part of the Hikurangi subduction

1148 margin, general section line illustrated on inset map. Regional tectonism adapted from

1149 Chanier et al. (1999); Bailleul et al., (2013); Reyners (2013) and Burgreen-Chan et al. (2016).

1150 International time scale after Cohen et al. (2013), New Zealand stages after Raine et al.
1151 (2015). Study intervals highlighted with dashed yellow boxes.

1152

1153 Fig. 3. A) Geological map of the onshore study area in the Akitio Basin (Heron, 2014), with
1154 mapped extent of the lobe complexes and the overlying mass-transport deposits (MTD)
1155 overlain on a shaded relief basemap. B) Cross-section of the Akitio Basin and adjacent
1156 structures; base of the studied Lower Miocene interval indicated with a dashed line. Modified
1157 from Lee and Begg (2002) and Malié et al. (2017). Note the simplified colours shown on the
1158 cross-section are representative of the general stratigraphy, as with Figure 1.

1159

1160 Fig. 4. A) Photo-mosaic of Owahanga Gorge northern side outcrop showing mostly
1161 amalgamated medium to thick-bedded sandstones (LF1), with subordinate laterally
1162 discontinuous thin-beds (LF3) of lithofacies association 1 (LA1). B) Close-up photograph of
1163 the laterally discontinuous thin-beds (LF3), hammer handle for scale is 20 cm long. C) Close-
1164 up photograph of thick-bedded, amalgamated sandstones (LF1). D) Photograph of incisional
1165 cuts and fills interpreted as a distributary channel fill (LF2). E) Logged section through a
1166 distributary channel or scour fill (LF2). F) Logged section through laterally continuous series
1167 of amalgamated sandstones (LF1). G) Logged sections of laterally discontinuous thin-bedded
1168 turbidites (LF3), laterally continuous thin-bedded turbidites (LF4), a rare hybrid event bed
1169 (LF5) and bioclastic grit (LF6). Log locations shown on log 1 in Figure 5.

1170

1171 Fig. 5. Logged sections L1 and L2 through the thick-bedded, amalgamated sandstones in the
1172 Owahanga Gorge (Fig. 3). Petrophysical data displayed for L2. Logged section L3 from the

1173 heterolithic overlying section. Inset map showing extent of lithofacies association 1 (LA1) in
1174 the Owahanga Gorge area, with the location of the three illustrated logs. Detailed logs and
1175 full petrophysical data are available in supplementary material; key to symbols in Figure 4.
1176 LC = lobe complex.

1177

1178 Fig. 6. A) Photo panel of lobe fringe (LA2) section in Pongaroa Stream. B) Interpretation of
1179 the outcrop, which is mostly composed of laterally continuous thin-beds (LF4), but with
1180 minor laterally continuous (LF1) and laterally discontinuous thick-bedded sandstones (LF2).
1181 C) Photo panel of the top of log L3, showing thin- to thick-bedded turbidites of LA2
1182 truncated and overlain by chaotic siltstones of LA3.

1183

1184 Fig. 7. Logged sections L4, L5, L6 and L7 through the Upper Burdigalian heterolithics on the
1185 western side of the Akitio Basin, LA2 as beige coloured map unit (Fig. 3). Note occurrences
1186 of thick mudstone intervals, e.g. at 47 m, 53 m and 57 m up log L7 and 32 m, 83 m and 116
1187 m up log L4. Mapped extent of lithofacies association 2 (LA2) in the western limb of the
1188 Akitio Syncline, showing location of the illustrated logs. Detailed logs and petrophysical data
1189 are available in supplementary material.

1190

1191 Fig. 8. Quantitative observations including a breakdown of sediment type, style of structures,
1192 palaeocurrents and bed thickness from A) Lithofacies association 1, dominated by tabular,
1193 thick-bedded, sandstones (LF1) intercalated with irregular thin-beds (LF3), lenticular, thick-
1194 bedded, sandstones (LF2) and rarely hybrid event beds (HEB; LF5). Amalgamated beds up to
1195 2 m thick traceable over 100's of m, in a unit 200 m thick and >5 km wide. Average net to

1196 gross 86%; foraminifera water depth mid bathyal (>700 m). Deposition from dominantly high
1197 to low-density, high-concentration turbidity currents, with bypass of finer suspension cloud
1198 particles due to flow stripping. B) Lithofacies association 2, laterally continuous thin-beds
1199 (LF4) with sporadic tabular thick-beds (LF1), separated by mudstones (LF7), hybrid event
1200 beds (LF5) and rare lenticular, thick-bedded, sandstones (LF2) in packages tens to hundreds
1201 of metres thick occurring across the sub-basin where LA1 not present. Average net to gross
1202 40%; foraminifera water depth mid bathyal (>700 m). Deposition from dominantly waning,
1203 low-density turbidity currents, periodically with influxes of higher concentration turbidity
1204 currents and flow transformations resulting in hybrid event debris flows.

1205

1206 Fig. 9. Petrophysical logs and correlation of logged sections L2 and L5, illustrating the
1207 development and correlation of seven lobe complexes. Age abbreviations as Fig. 2. LC = lobe
1208 complex.

1209

1210 Fig. 10. Top: Non-interpreted dip profile seismic cross-section of the Porangahau Trough and
1211 Ridge (see location in Fig 1, respectively PT and PR). Bottom: Interpreted section
1212 highlighting the evolution of the basin fill and structures. Seismic facies 1 represents the
1213 background, non-shaded intervals. SA = Seismic facies associations. Note 2x vertical
1214 exaggeration.

1215

1216 Fig. 11. (A) Detailed seismic dip line across the Porangahau Trough (PT) and Porangahau
1217 Ridge (PR). (B) Interpretation of dip line. (C) Strike line along the Porangahau Trough. (D)
1218 Interpretation of strike line. (E) Dip line from (A) flattened on base lobes (SF4). (F)

1219 Interpretation of flattened lobes and MTDs (SA2). (G) Dip and strike lines, and depth slice of
1220 basal lobe complex. (H) Interpretation of G (SA2). Note dip and strike lines intersect in the
1221 middle of the view. Seismic facies 1 represents the background, non-shaded intervals. SA =
1222 Seismic facies associations. Note 4x vertical exaggeration in A-F.

1223

1224 Fig. 12. A) Root-mean-square (RMS) amplitude horizon along the studied subsurface
1225 Madden channel – lobe system, highlighting the otherwise low amplitude response across the
1226 margin during the study interval. The detailed area, linked cross-sections of the Porangahau
1227 Trough (PT), Ridge (PR) and the next downstream basin, and step by step horizons is shown
1228 in B-G, which represent ca. 50 m intervals through the lobe system, a systematic view
1229 through all reflectors is provided in the supplementary video. B) Below the lobe complexes,
1230 with feeder channel supplying sediment into a fully ponded and silled basin. C) First lobe
1231 complex developing at mouth of feeder channel; note subsequent erosion within the channel,
1232 likely related to later MTD emplacement excising an up-dip portion of the lobes. D) Second
1233 lobe complex, displaying distributary channels. E) Third lobe complex; up until this point the
1234 bypassing fines are inferred to be below seismic resolution but from here on a gradual
1235 brightening of the downstream basin is seen. F) Upper lobe complex, displaying lower RMS
1236 response and potential spill of fine-grained material into the downstream basin and erosion of
1237 the sill crest. G) Termination of the lobe system by emplacement of a low amplitude (muddy)
1238 mass-transport deposit (MTD). Maps are displayed so as low amplitude reflectors (i.e., fine-
1239 grained deposits) are in dull black to grey colours whilst the high amplitude (i.e., coarser
1240 grained deposits) are displayed in bright colours.

1241

1242 Fig. 13. Cross-plot of lobe system thicknesses and lengths from a range of deep-water lobes
1243 across the globe. Other than results from this study, data was extracted from Flood et al.
1244 (1991); Horine et al. (2000); Pirmez et al. (2000); Piper and Normark (2001); Popescu et al.
1245 (2001); Grecula et al. (2003); Sixsmith et al. (2004); Van Lente (2004); Deptuck et al. (2008);
1246 Jegou et al. (2008); Iorio et al. (2009); Bourget et al. (2010); Figueiredo et al. (2010, 2013);
1247 Pringle et al. (2010); Flint et al. (2011); Brunt et al. (2013); Lericolais et al. (2013); Burgreen
1248 and Graham (2014); Yang and Kim (2014); Hofstra et al. (2015); Tinterri and Tagliaferri
1249 (2015); Zhang et al. (2016); Dennielou et al. (2017); Jobe et al. (2017, 2018); Liu et al.
1250 (2018); Postma and Kleverlaan (2018); Pyles et al. (2019); Tinterri and Piazza (2019).

1251

1252 Fig. 14. Schematic flow process and kinematic model for sediment – structure interaction
1253 from time 0 – 4. Initially sediments entering the basin pond within the centre, onlap edges
1254 and intra-basinal structures (T0). Subsequent sediment influx supresses intra-basinal
1255 structures, focusing stress on basin-bounding structures (T1-3). If the growth of Thrust 1 [F1]
1256 and Thrust 2 [F2] are similar and the net sediment flux [S] balances the rate at which
1257 accommodation space is generated (by tectonic [T] and isostatic loading [L]) then
1258 aggradationally-stacked lobe complexes (LC) may develop. Under this scenario dynamic
1259 growth of basin-bounding structures maintain sills and perpetuate flow stripping, trapping
1260 coarse material behind the down-slope sill, whilst allowing downstream bypass of fines. This
1261 equilibrium is eventually disrupted by allogenic factors, here being emplacement of a
1262 regional mass-transport deposit.

1263

1264 Fig. 15. Schematic tectono-stratigraphic evolution model of trench-slope basin fill. A-C show
1265 allogenic control by flow stripping at the downstream sill, resulting in trapping of coarse-

1266 grained lobe systems behind the sill with bypass of fine-grained particles downstream. D)
1267 Ultimately, an autogenic influence (here emplacement of a mass-transport deposit) results in
1268 fundamental modification of the sedimentary system, basin dynamics and disrupting the
1269 balance between sedimentation and deformation.

1270

1271 Fig. 16. Schematic Gamma Ray (GR) wireline log motifs and composite (Comp) logs for a
1272 lobe complex fringe, axis, bypass edge and downstream basin. Note bypass thin beds are not
1273 laterally extensive and may not present a barrier to fluid flow, unlike the blanketing fines of
1274 the fringe or downstream basin.

1275

SUPPLEMENTARY MATERIAL CAPTIONS

1276 A. Detailed sedimentary logs 1-7. Log 1 location start 176.2732, -40.6301; finish
1277 176.2741, -40.6254. Log 2 start 176.2774, -40.6275; finish 176.2758, -40.6250. Log 3
1278 coordinates start 176.2727, -40.6214; finish 176.2744, -40.6206. Log 4 start
1279 176.2194, -40.5547; finish 176.2236, -40.5611. Log 5 176.2162, -40.5565. Log 6
1280 176.2221, -40.5638. Log 7 start 176.2212, -40.5557; finish 176.2260, -40.5588.

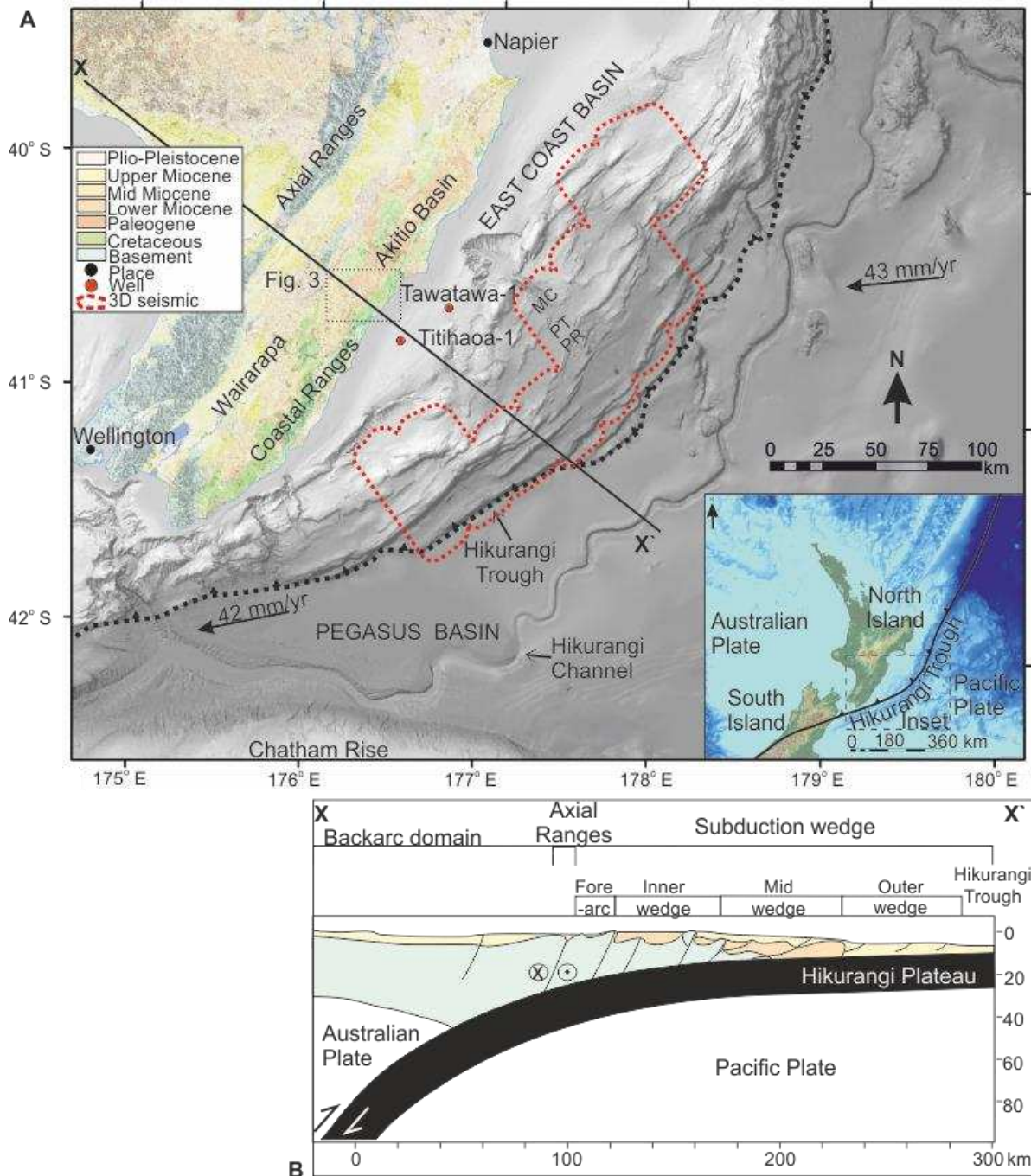
1281 B. Gamma Ray and clay minerals data from logged sections L2 and L5.

1282 C. Video of all mapped horizons, from the subsurface example. Video covers from
1283 emplacement of lower MTD, through the higher amplitude lobe complexes to the
1284 termination of the lobe system by emplacement and incision by the upper MTD.

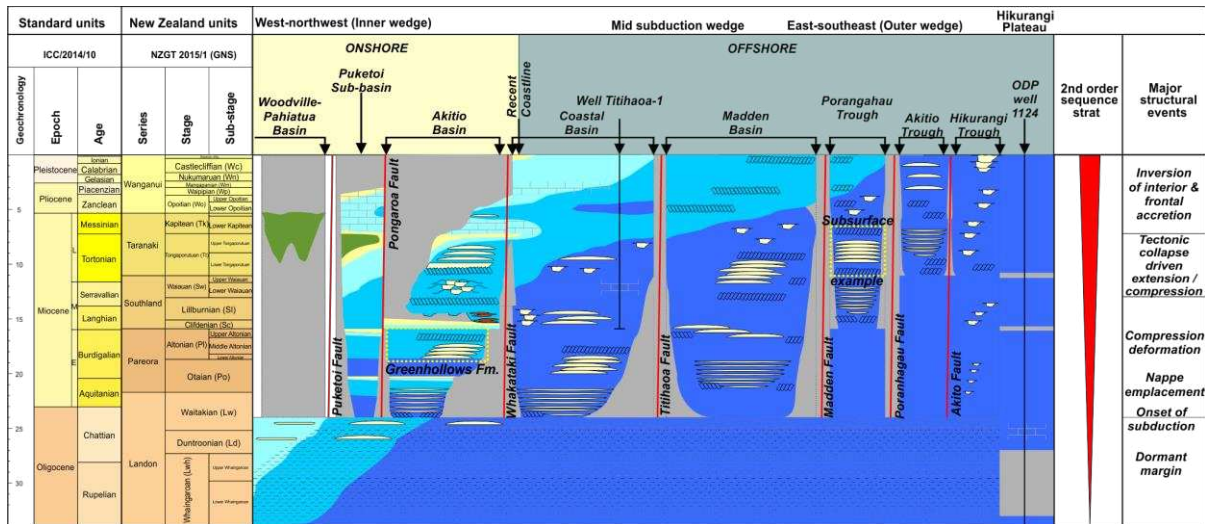
1285

1286

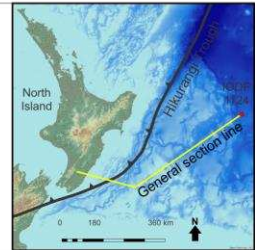
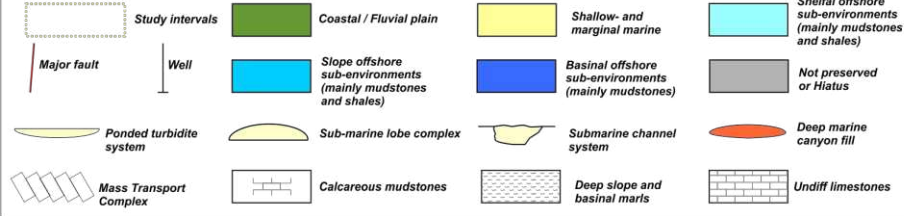
1287



1288



LEGEND

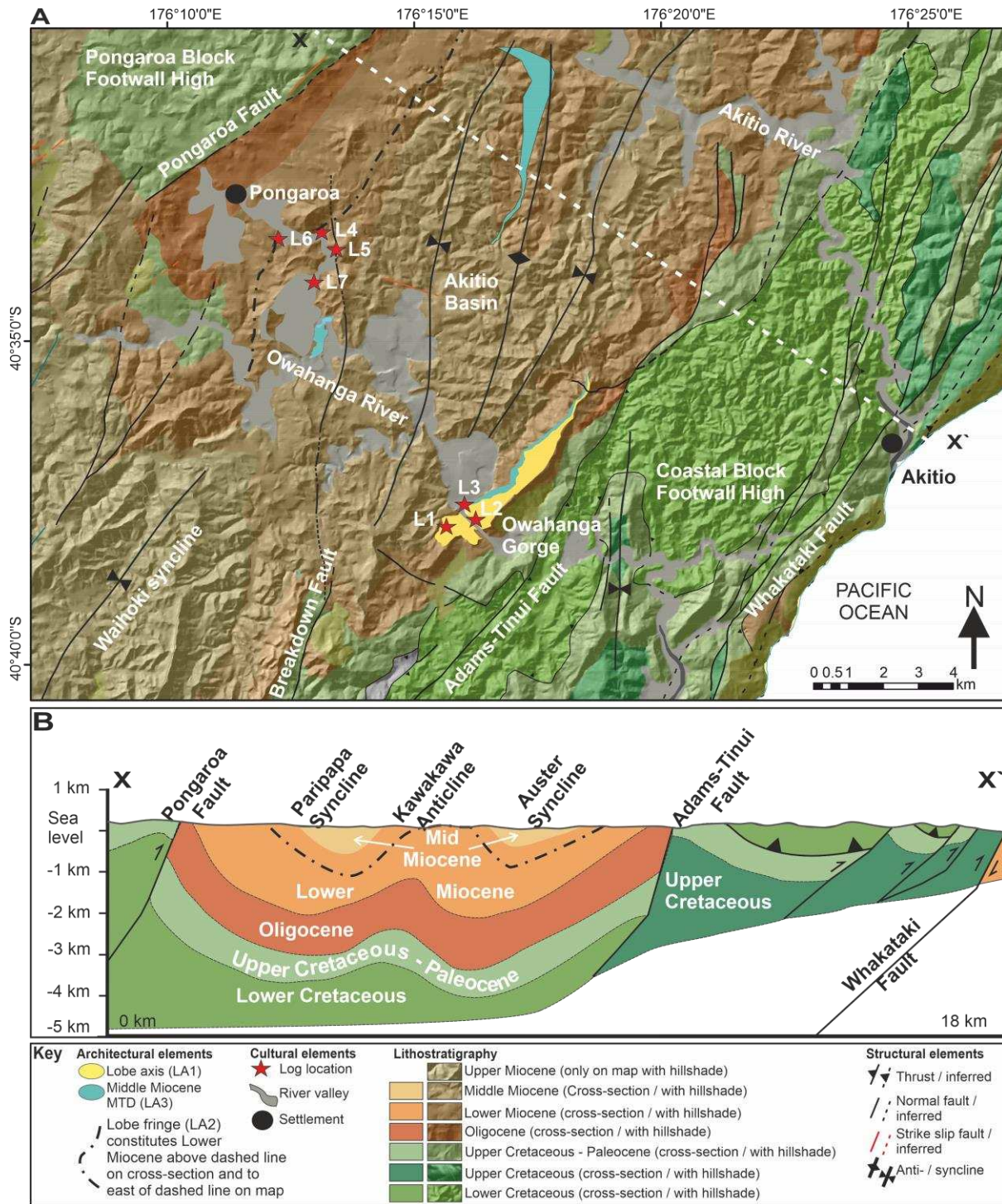


1289

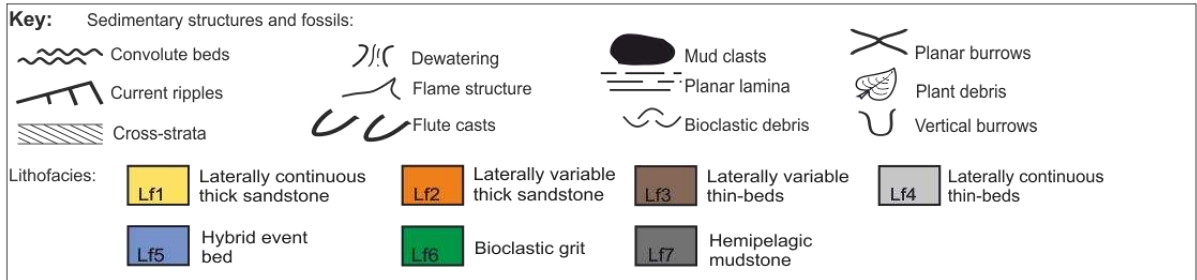
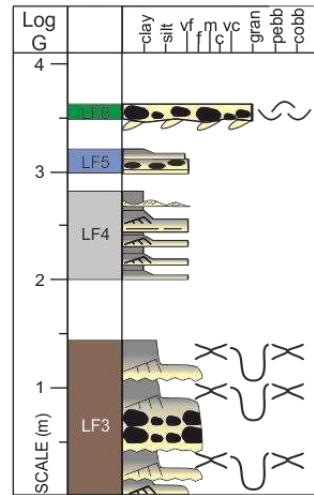
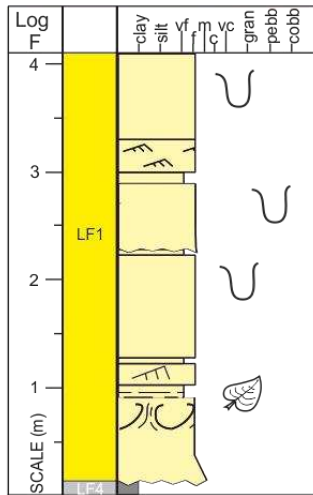
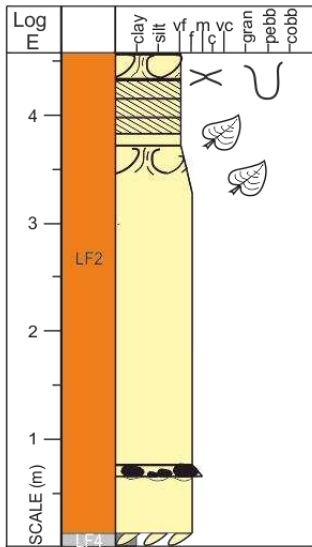
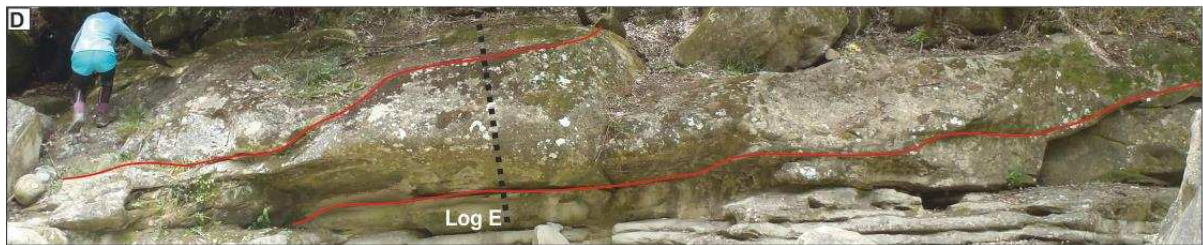
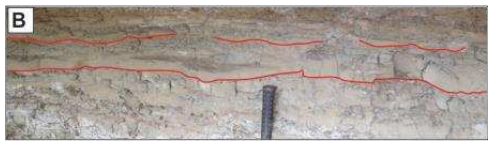
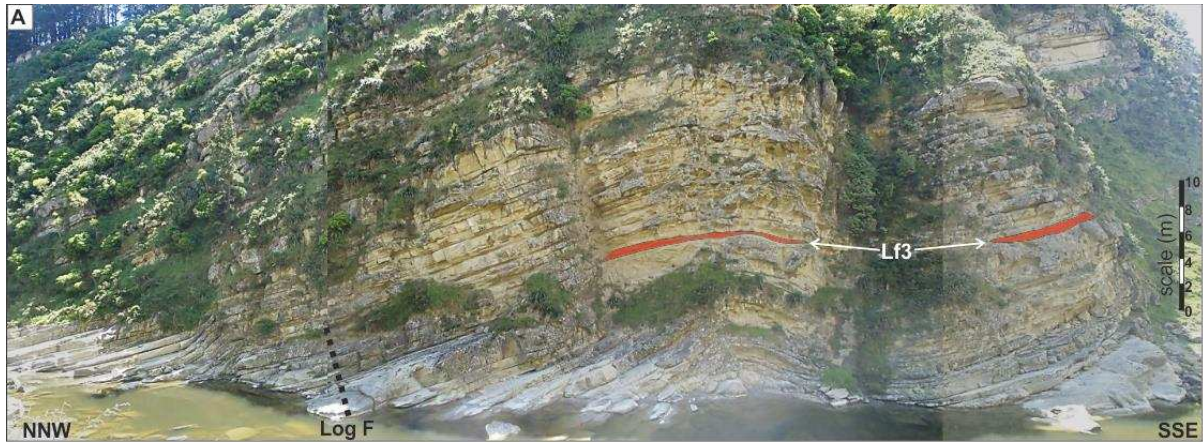
1290

1291

1292

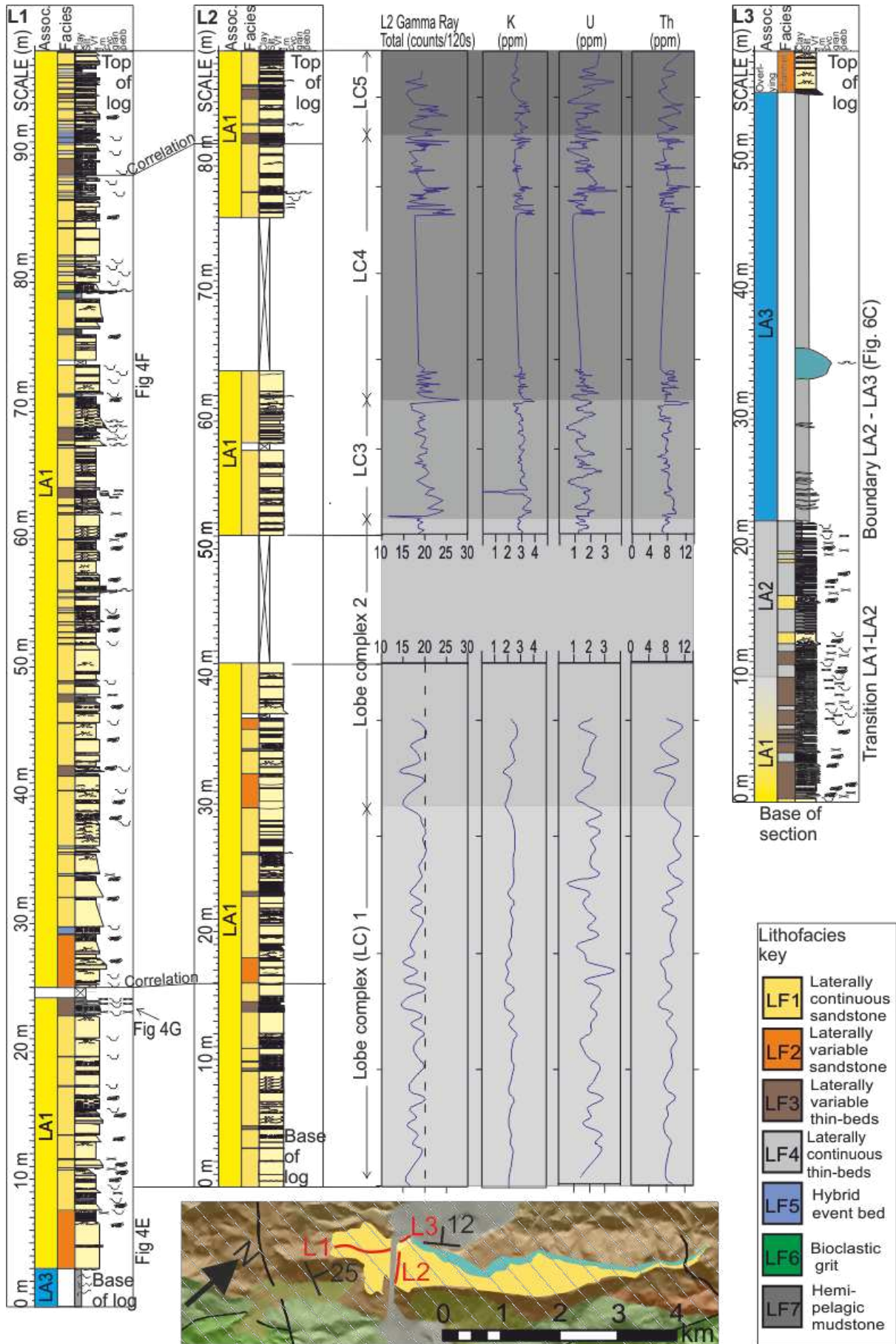


1293



1294

1295

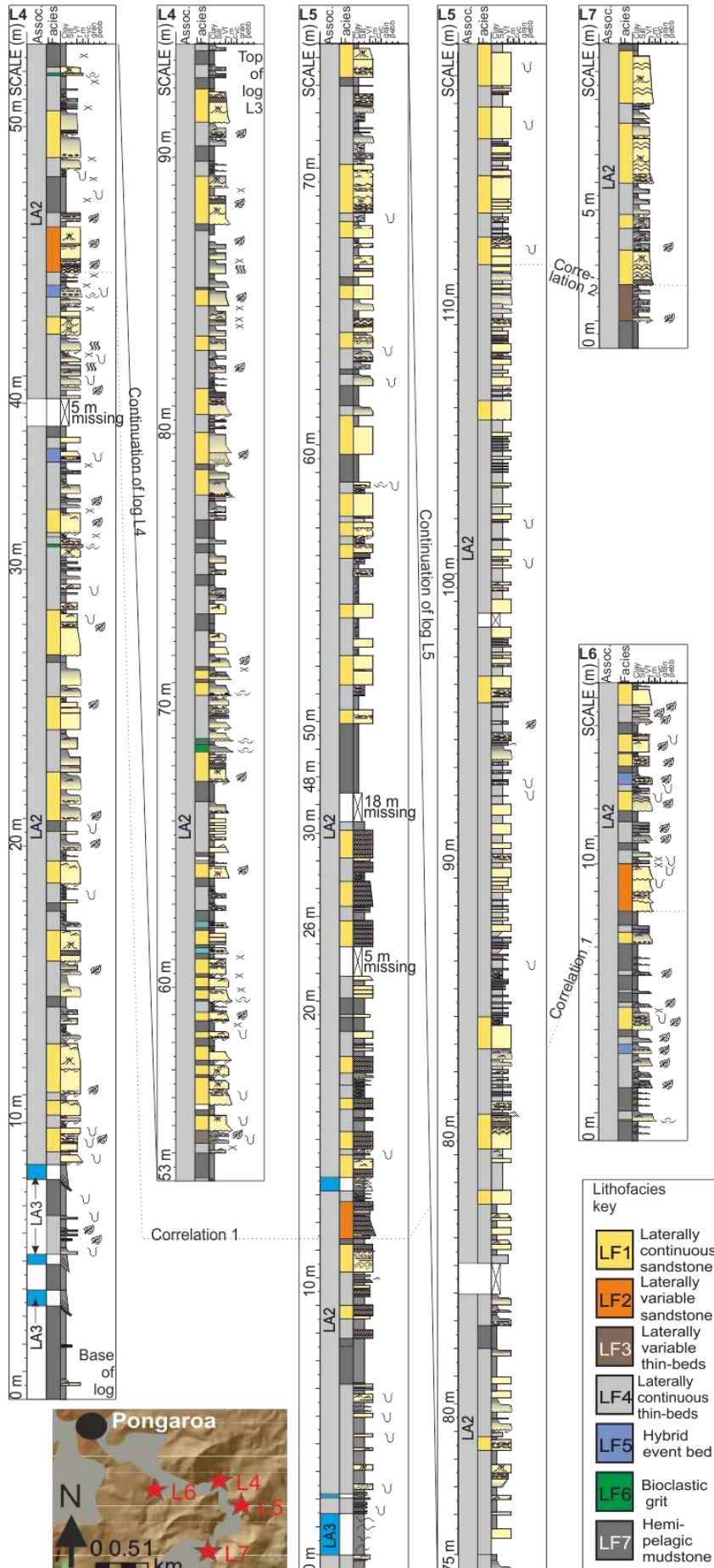


1297

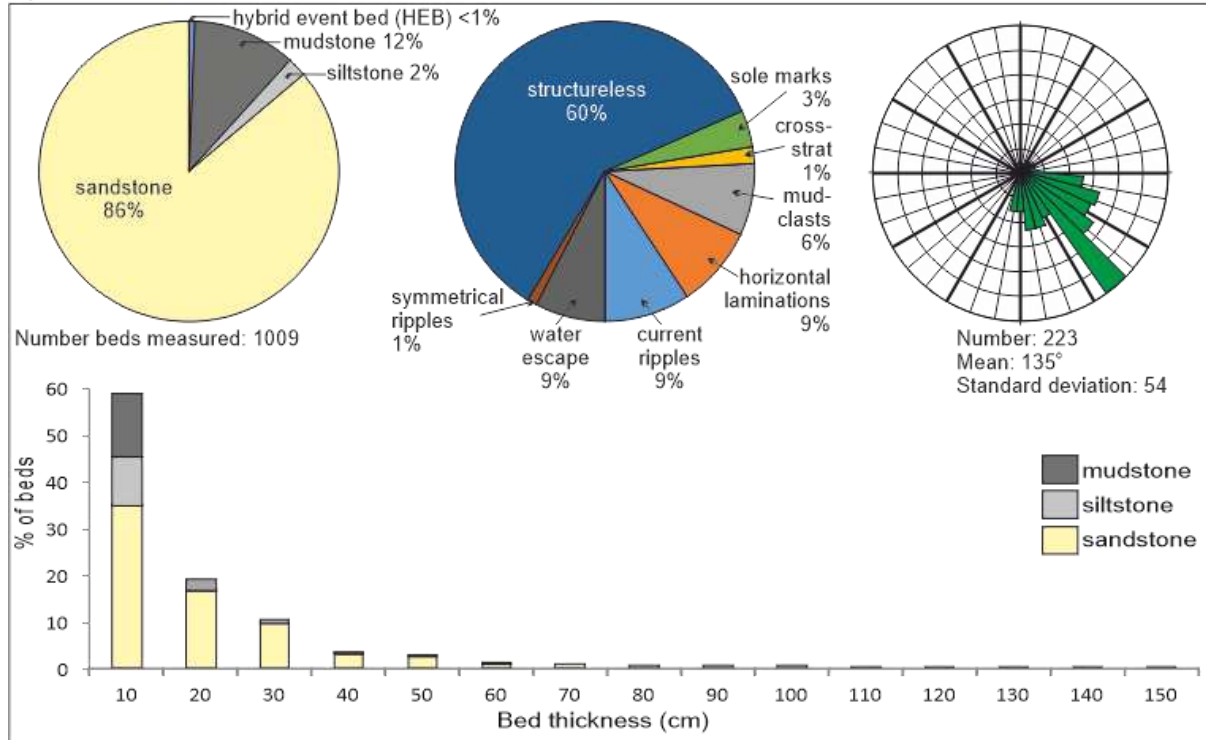


1298

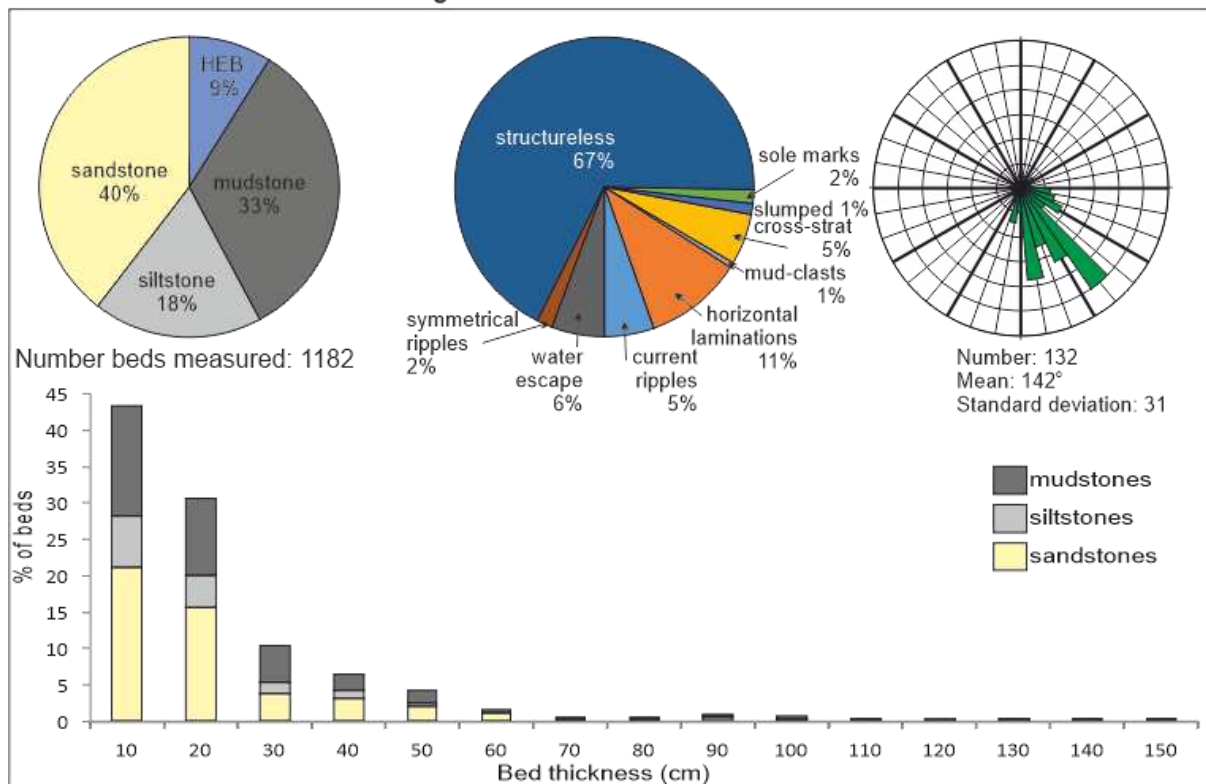
1299



A) Lithofacies association 1 - lobe axis

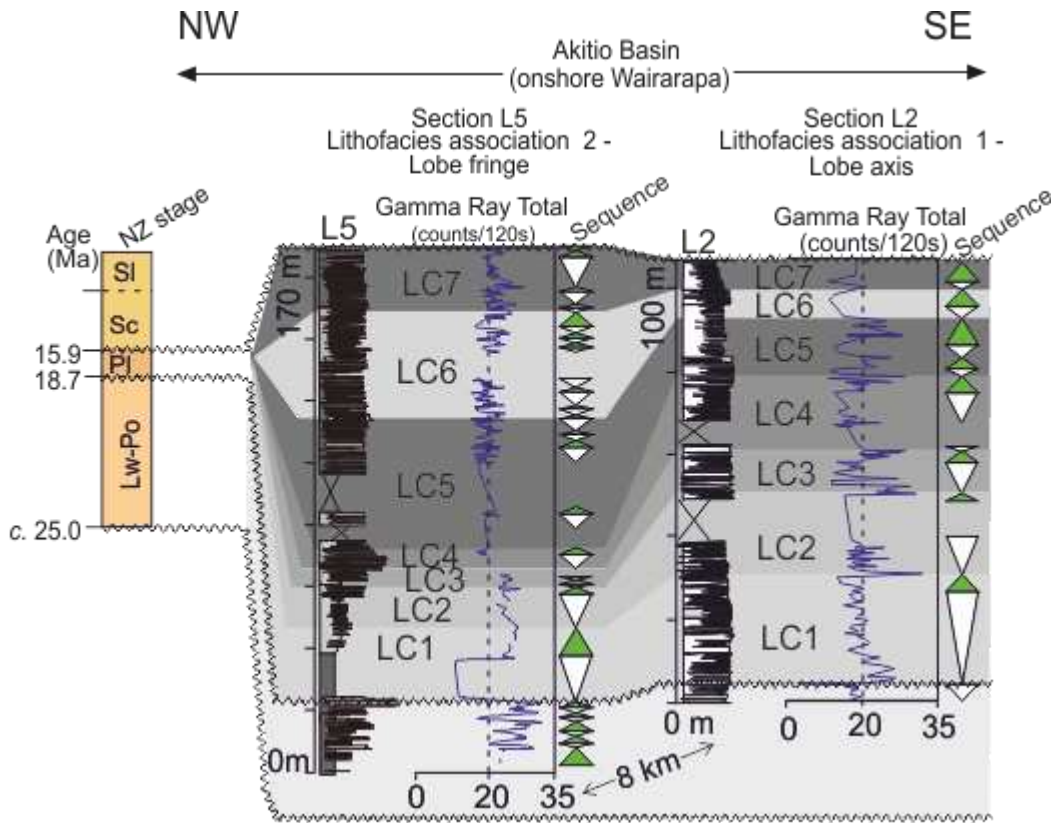


Lithofacies association 2 - lobe fringe



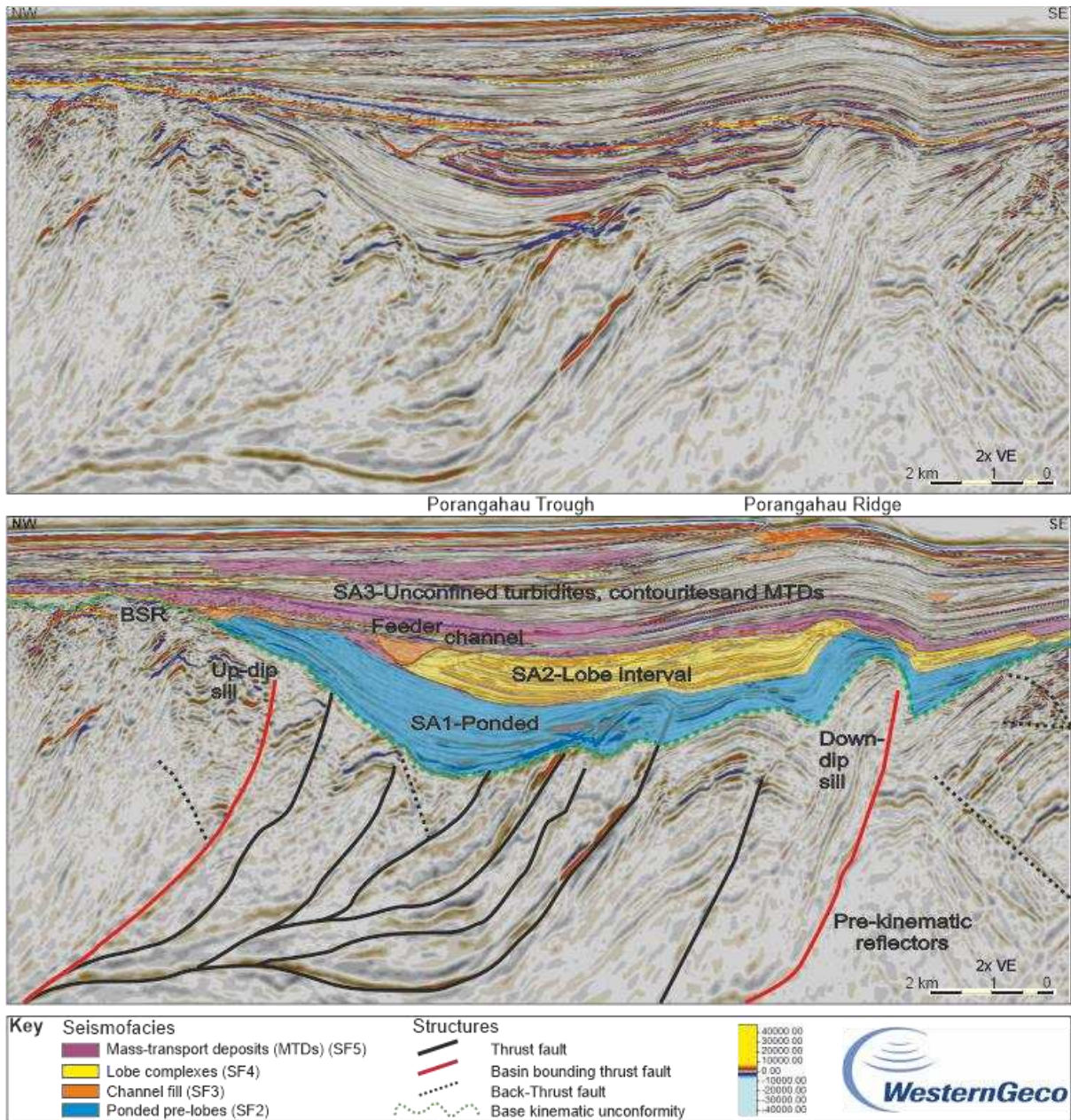
1301

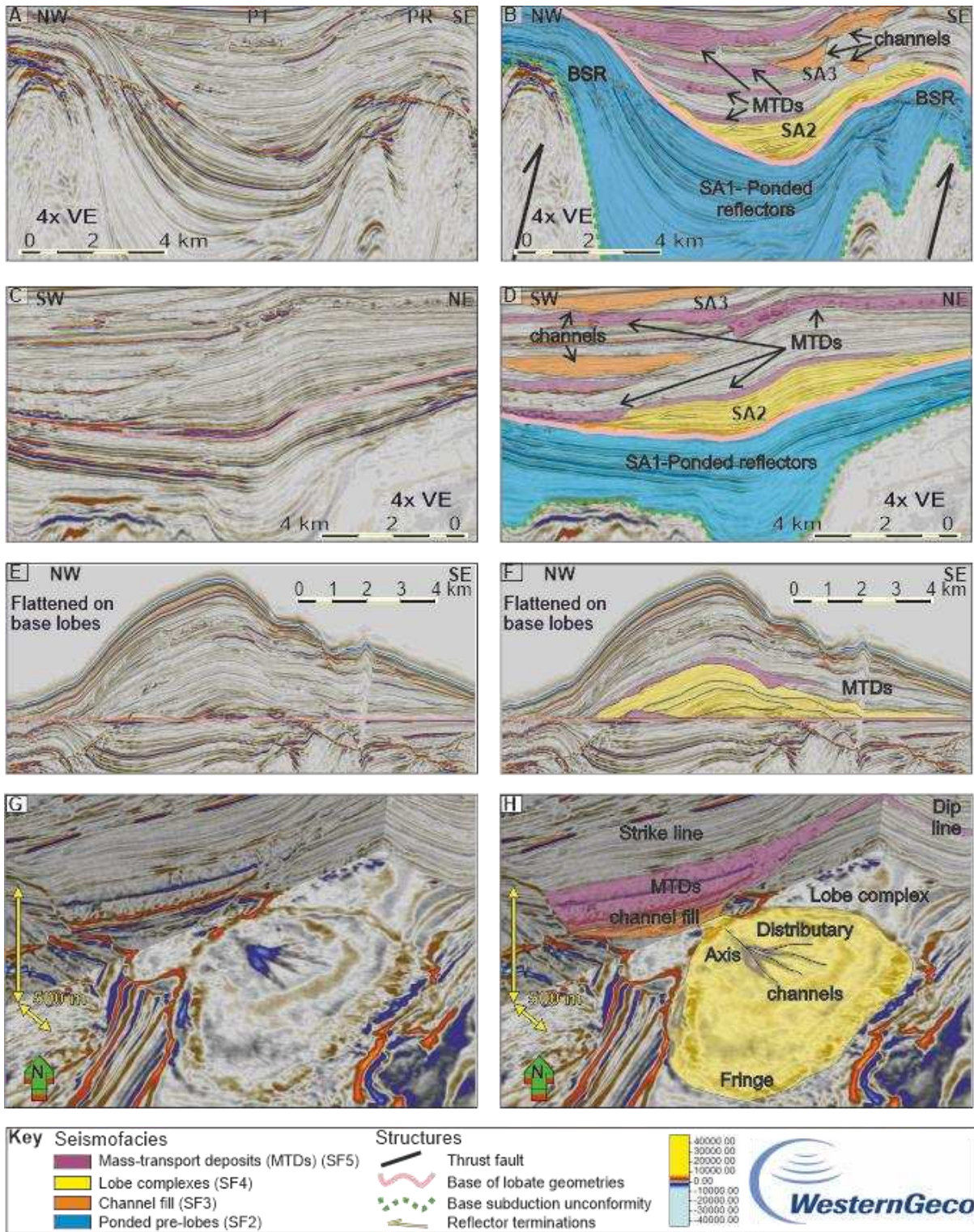
1302



1303

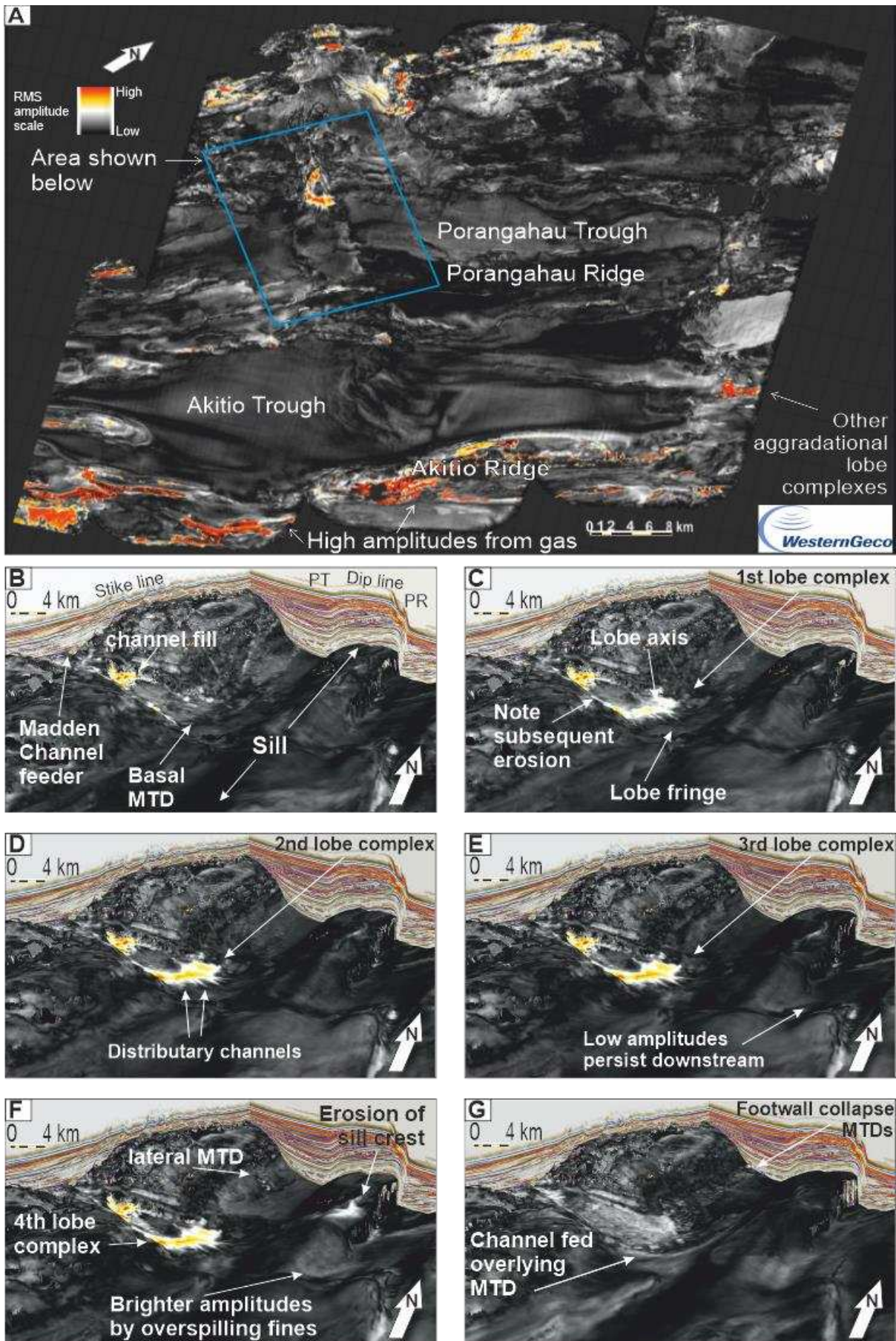
1304





1307

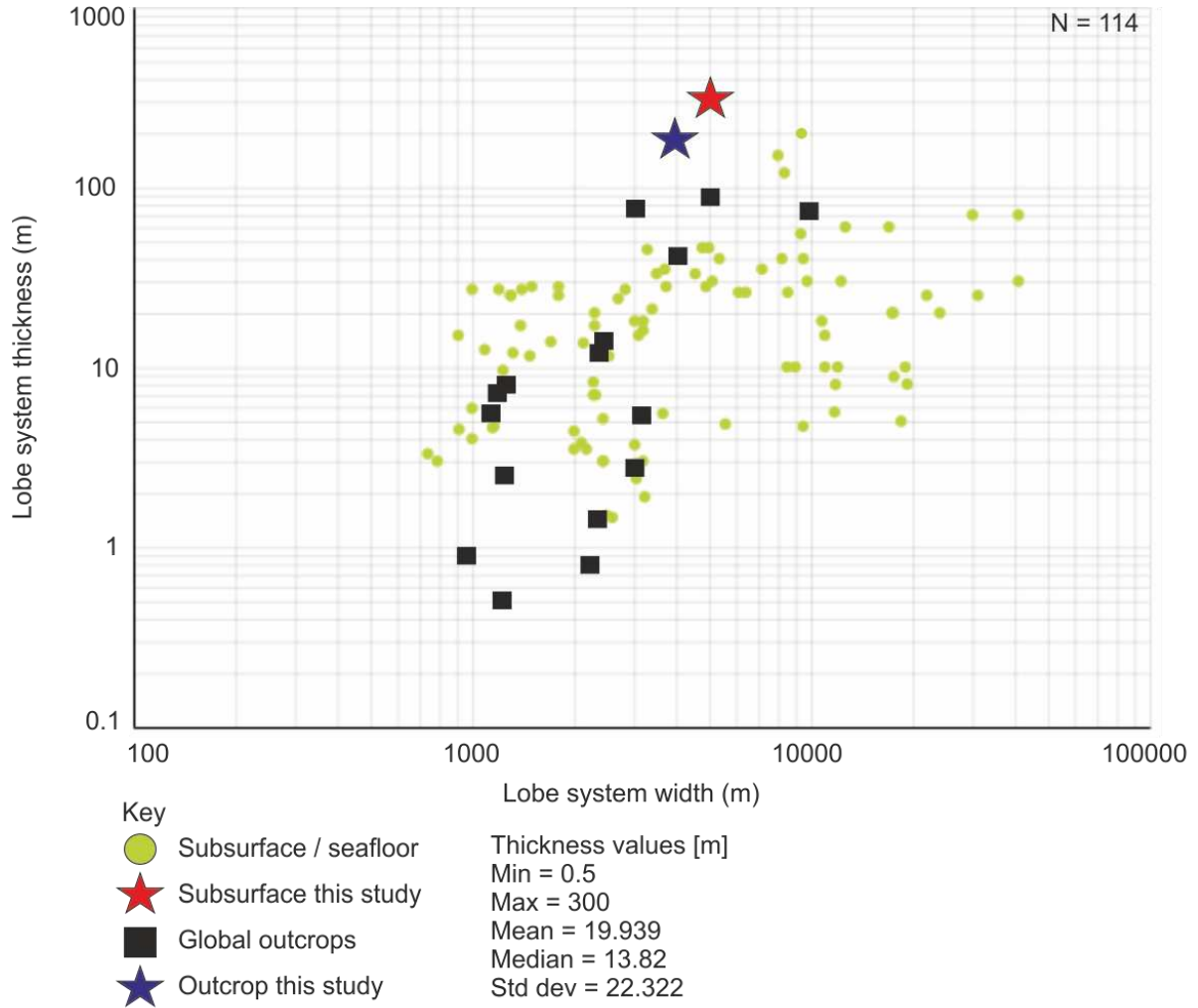
1308



1310

1311

1312

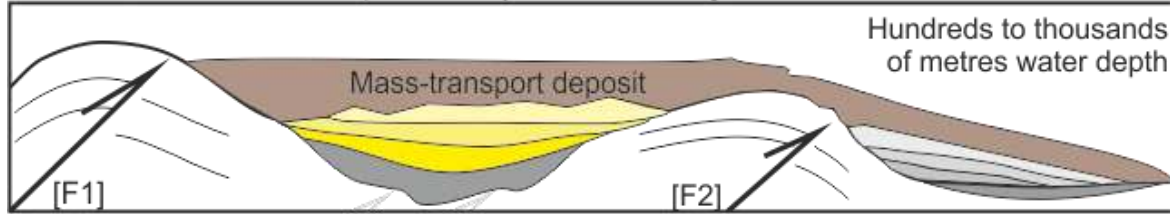


1313

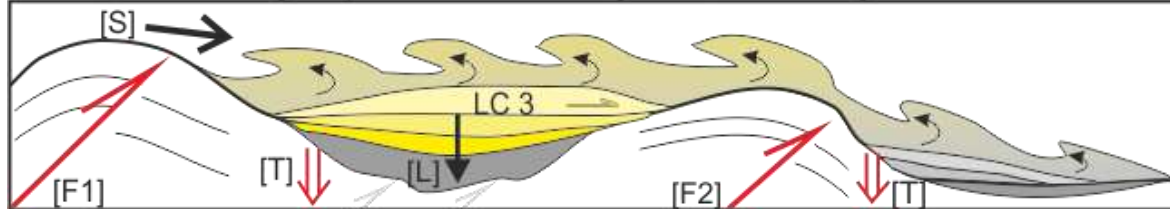
1314

1315

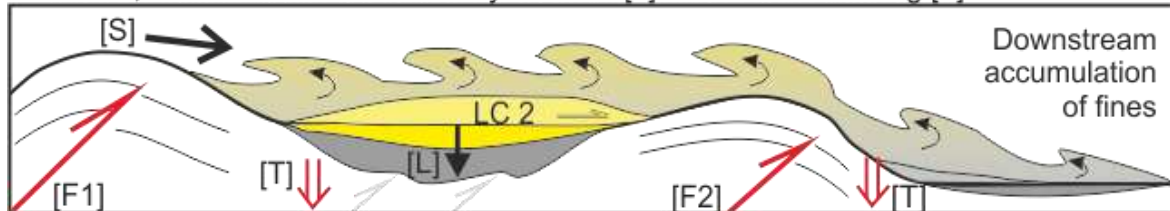
E: Time 4, Termination of equilibrium by external forcing



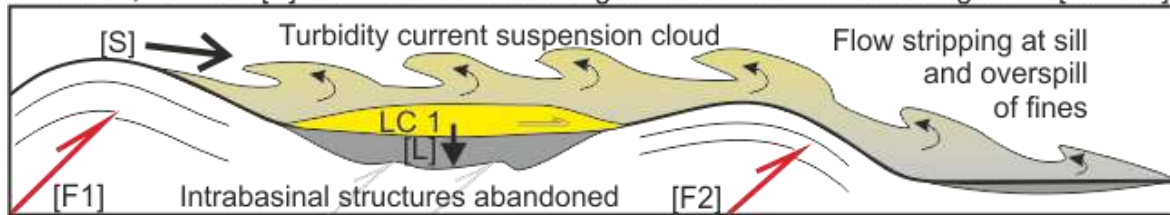
D: T3, Further loading keeps stress on bounding faults, maintaining flexure and subsidence



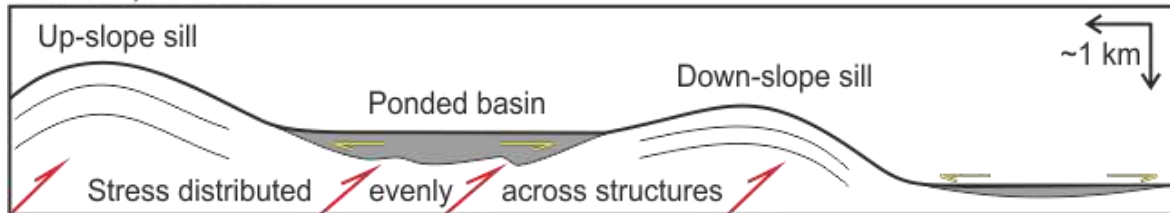
C: Time 2, Basin subsidence driven by isostatic [L] and tectonic loading [T]



B: Time 1, Sed flux [S] causes isostatic loading focuses stress on bounding faults [F1 & F2]



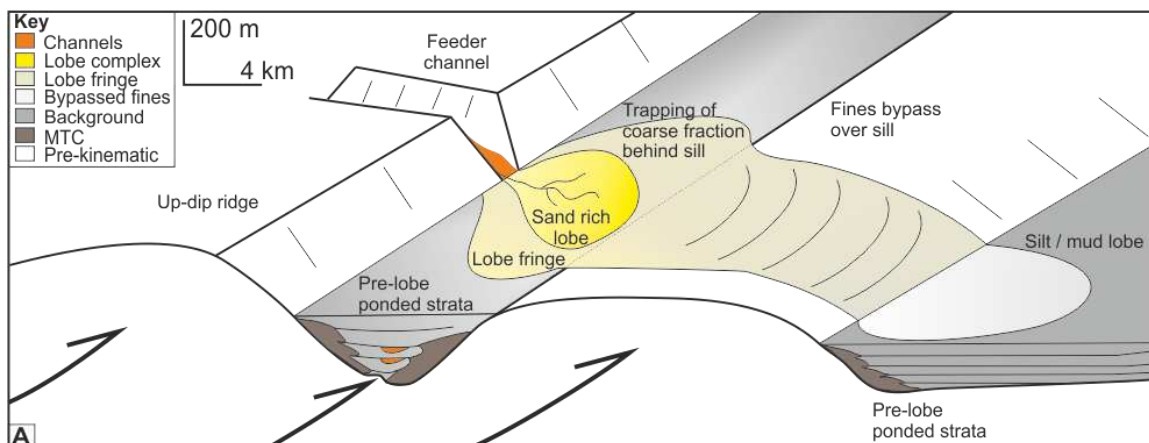
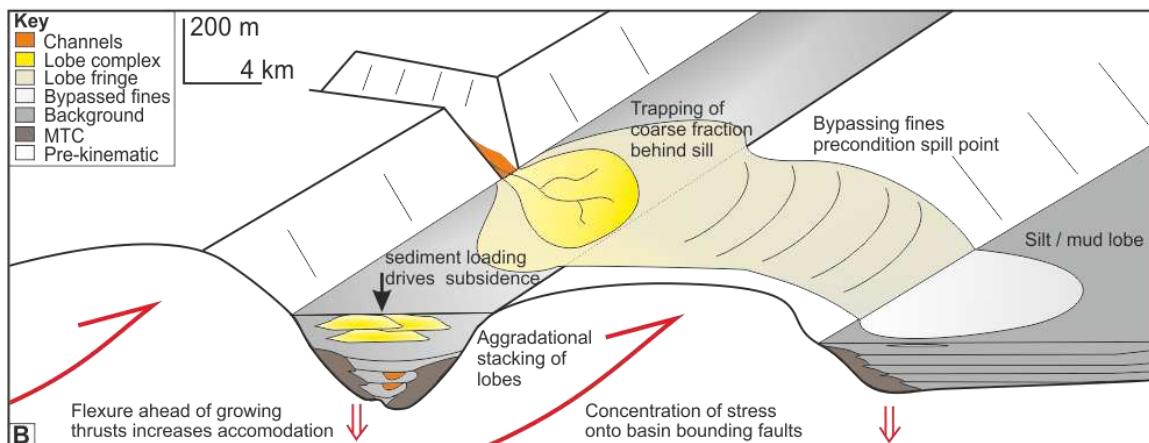
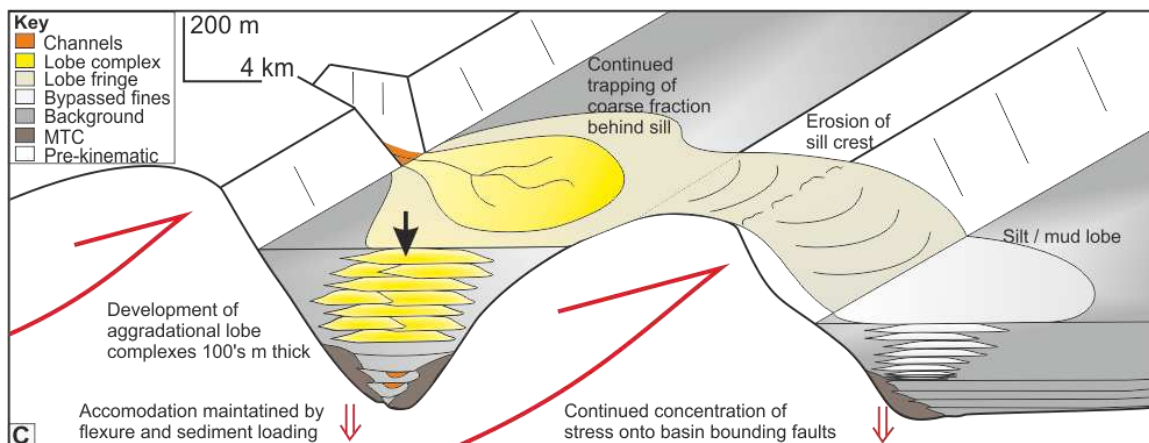
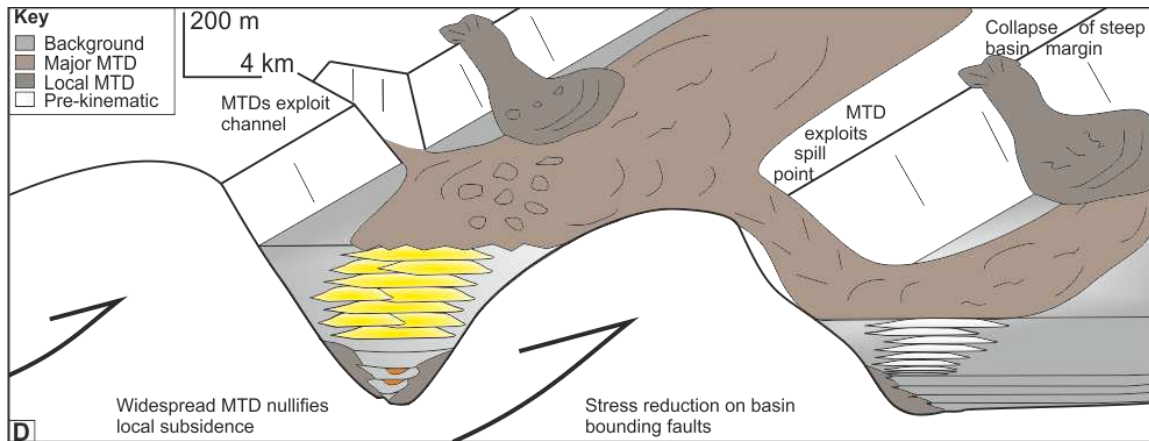
A: Time 0, Pre-lobes

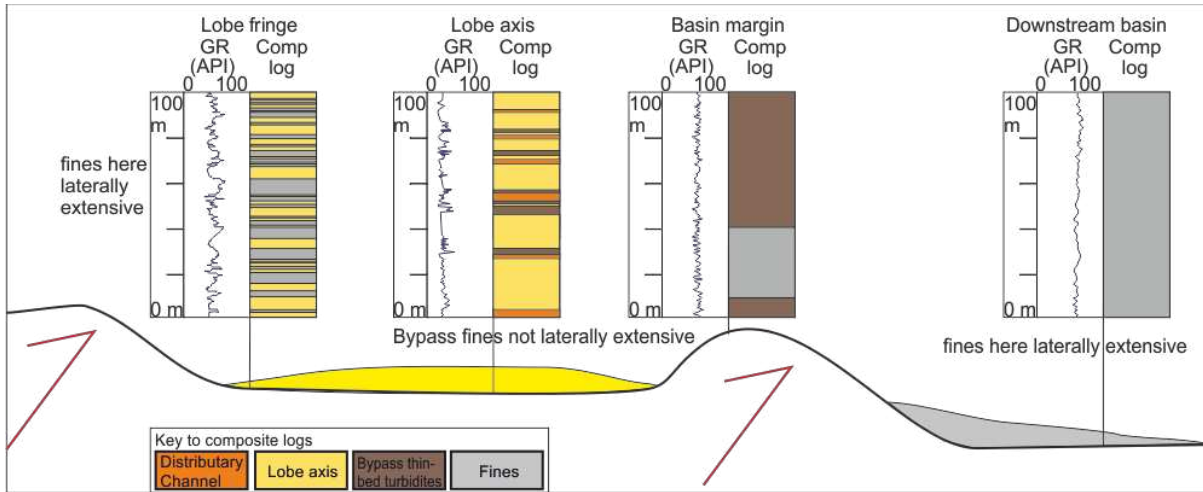


1316

1317

1318





1320

1321

1322

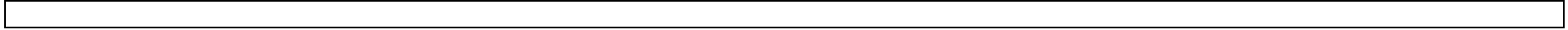







Table 1. Principal lithofacies types of the Greenhollows Formation examined in the present study.

	<p>Lithofacies 1: Tabular, medium to thick-bedded sandstone Description: Pale grey to beige, graded beds up to 2m thick of fine to very fine-grained, well-sorted sandstone. Bed bases are typically irregular and may truncate underlying strata by up to 10 cm; sole marks, primarily flutes are common. The bases may initially show inverse grain size grading. The lowermost portion (lower 5-10 cm) of beds may show planar lamination, often highlighted by carbonaceous bands, but planar cross-stratification was also observed. Above this the beds are typically massive and or dewatered. The upper portion may show a return to planar and ripple lamination. This is an idealised succession and beds may show a different order or not all of the structures. Variably sole marks, cross-strata and ripples may show subtly different orientations (Fig. 8). Sandstones are often amalgamated; rare trains of internal mud-clasts or grain size breaks may mark amalgamation surfaces. Mud-clasts may also occur scattered throughout individual beds. These beds are tabular and may be traced over tens to hundreds of meters across any one outcrop.</p>	<p>Interpretation: These sandstones are interpreted as the deposition from high to low-density, high-concentration turbidity currents (sensu Lowe, 1982), with current re-working. Massive portions were likely deposited under upper stage flow regimes, with high sediment fallout rates, but could also have lost structures due to dewatering; both processes indicating rapid deposition. Cross-strata, the thickness of beds and climbing ripples imply sustained flows. Waning flows may have resulted in the gradational upper portion of beds (Bouma Tacc). Variations in palaeocurrent indicators is interpreted as a result of sediment transport in a confined setting, with deflections in the flow (sensu Kneller and McCaffrey, 1999). Bed amalgamations, inverse grading of the lower portion and missing fractions imply a proportion of these flows were bypassing and mud-clasts imply these flows had the ability to erode the sea-floor.</p>
	<p>Lithofacies 2: Lenticular thick-bedded sandstone Description: Pale grey to beige irregularly bedded fine-grained sandstones up to 3 m thick. Bed bases are irregular, with decimetre scale incisions truncating underlying strata. Sole marks, primarily flute casts may scour into the underlying sediment. Beds variably show planar cross-stratification, extensive dewatering and convolute bedding, grading to planar lamination and ripple lamination at the bed tops or may be massive and contain abundant sand- and mud-clasts. Laminations are often highlighted by organic rich bands and carbonaceous debris up to 10 cm long. Amalgamation is common and beds typically show a lenticular form, thinning over tens of meters in width. Rarely beds are granular to medium grained and may have a significant glauconite and bioclastic component. Bioturbation is rare and occurs as large vertical burrows (e.g. <i>Ophiomorpha</i> sp.) at bed tops and fossils were only observed as broken shell fragments <1 cm.</p>	<p>Interpretation: These relatively coarser grained, often cross-stratified, lenticular beds are interpreted as the fill of low aspect ratio scours and / or small distributary channels by deposits of high-density turbidity currents (Normark et al., 1979). The structures and fill imply channel fills are the more likely (e.g. Kane et al., 2009; Prelat et al., 2009). The bioclastic and glauconitic bed bases implies that at least part of these flows initiated in a shallow marine environment, however the fact that the upper portions of these beds commonly show carbonaceous material and carbonized wood fragments implies some terrigenous mixing.</p>

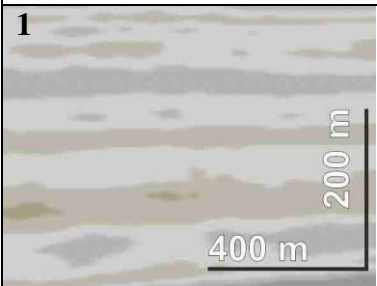
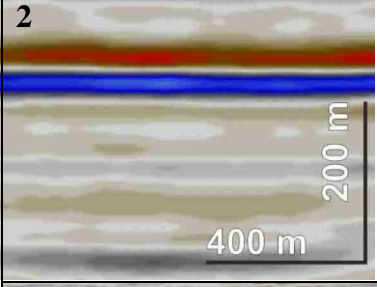
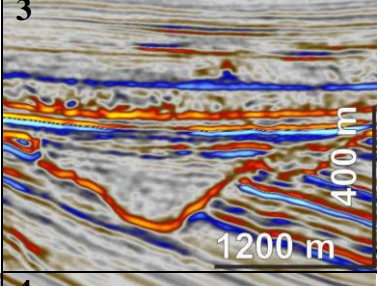
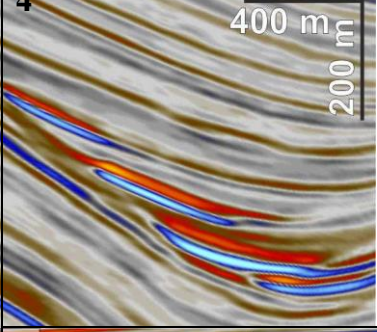
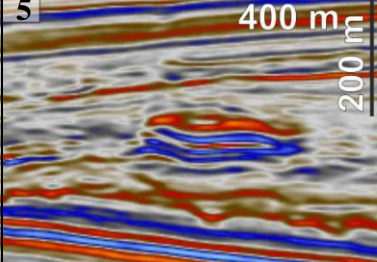
	<p>Lithofacies 3. Discontinuous thin- to medium-bedded sandstones and siltstones Description: Pale grey to beige, well sorted, fine to very fine-grained sandstones overlain by siltstones, typically < 10 cm thick. Typically shows a sharp, irregular base, occasionally lower portion of beds show planar laminations and upper portions may show ripples and cross-lamination with siltstone. Beds are not necessarily normally graded and may show variation in the order of structures. Beds may show significant lateral variation in thickness, occurring as lenses, pinching-and swelling or thinning laterally. May be rich in carbonaceous material. Sandstones are typically texturally immature, displaying a variety of lithic fragments and glauconite. Bioturbation is variable but macrofossils were not observed.</p>	<p>Interpretation: Deposition from dilute, low-density turbidity currents (Bouma Tc-d-e). The presence of traction structures implies deposition from waning flows. The lateral variation may be a result of thinning and pinch out against a confining surface when apparent or to have infilled a scour surface. When filling scours these deposits may be inferred to have a bypass component, especially when grain size fractions are missing (<i>sensu</i> Stevenson et al., 2015).</p>
	<p>Lithofacies 4: Tabular thin- to medium-bedded sandstones, siltstones and mudstones Description: Pale grey to beige, normally graded, typically well-sorted, fine to very fine grained sandstones typically <20 cm thick. Bed bases may be sharp or slightly irregular with sole marks including tool marks and flutes. The lower portion of beds may show planar lamination, often highlighted by carbonaceous rich bands; beds typically subtly grade up and often show a dewatered and or massive middle interval; bed tops are typically current rippled and grade to siltstone and mudstone; this is an idealised succession and beds may show a different order or not all of the structures. Ripples often show a subtly different orientation to sole structures and infrequently show variations between rippled horizons in the same bed (Fig. 8). These beds are tabular and may be traced over hundreds of meters across any one outcrop. Bioturbation is variably absent to intense, particularly in bed tops which may show a mottled texture.</p>	<p>Interpretation: These sandstones that grade to silt- and mudstones, with a variety of traction structures are interpreted as the deposition of fine grained sediments from low-density turbidity currents (Bouma Tb-c-d-e). The normal succession of structures and continuity of beds implies deposition from waning flows. Variations in palaeocurrent indicators is interpreted as a result of sediment transport in a confined setting, with deflections in the flow (<i>sensu</i> Kneller and McCaffrey, 1999).</p>

	<p>Lithofacies 5: Alternation of sandstones and debrites Description: In idealized sections immediately overlying thin-bedded (<10 cm), very fine-grained, often rippled horizons of “clean” sandstone, are medium bedded (20-60 cm) argillaceous sandstones, rich in floating mudstone clasts (up to 60%). Clasts are typically <20 cm long and less than 5 cm thick, sub-spherical and sub-elongate, but become more angular and elongate with increased size. These deposits are matrix supported, which normally consists of a “dirty” sandstone, rich in micaceous material, organic matter and occasionally bioclastic debris. These are typically overlain by a thin, argillaceous sandstone, although the overlying sandstone may be truncated by a subsequent deposit.</p>	<p>Interpretation: These sandwich beds are interpreted as hybrid event beds, <i>sensu</i> Haughton et al. (2003). The Initial clean sandstone may represent the head of the flow, which outran the erosive body, whilst delaminating the sea floor and entraining mud-clasts. This resulted in the body of the flow being deposited as a mud-clast rich debrite, over which the tail of the flow deposited a second, argillaceous sandstone. This is an idealised succession and all or parts of the event bed may be present depending upon run out distance, preservation etc.</p>
	<p>Lithofacies 6. Bioclastic grits Description: Pale yellow to beige, often weathering orange thin-beds of granular to fine material, primarily comprising a poorly sorted mixture of siliciclastic, bioclastic and glauconite grains of variable proportions. Mud-clasts are also common, typically less than 5 cm long, but up to 50 cm. Exotic pebbles are a rare inclusion. Bed bases are typically sharp, erosive and may display sole marks. Beds are variably massive, show coarse laminations or planar cross-stratification. Beds are often very laterally variable in thickness, grain size and persistence, often seen to be pinching and swelling down dip. Bioclasts include mollusc fragments, foraminifera, bone material (primarily fish, but also cetacean), corals and other marine organisms. Although rare, terrestrial material, including wood fragments may also be found in these beds. These beds may occur in isolation within mudstone intervals, or more commonly immediately below much finer grained LF1, 3 and 4, or very rarely as lamina in normally graded beds.</p>	<p>Interpretation: These coarse, bioclastic beds are interpreted as the deposits of gravity flows originating from local shallow marine environments, reworking material from shelves to deposit them in relatively deep-water. Their common association with very fine grained material may be interpreted in one of two ways. 1) These beds were triggered simultaneously with finer siliciclastic rich events. Or 2) They represent a missing grain size (bypassed) portion in normally graded events. The observation of beds grading normally through medium and fine with decreasing bioclastic content implies the latter was the dominant process. These beds have been proposed as possible marker horizons across the basin by (Francis and Johansen, 2011)</p>

	<p>Lithofacies 7. Massive, marine mudstone Light to dark grey mudstone occurring in beds up to 75 cm thick, which can amalgamate into packages meters to tens of meters thick. Beds are typically laterally continuous over outcrop scale. Bedding may be recognised by broad colour changes and concreated horizons. Rarely isolated silt- or sandstone lamina may occur. Typically exhibits a blocky texture, with a conchoidal fracture. Rarely shows small biocoenotic macrofossils, such as <i>Inerocamerus</i> sp. molluscs or macro foraminifera (e.g. <i>Bathysiphon</i> sp.). Rare fragments of organic matter are often disseminated and it may show bioturbation, with horizontal burrows such as <i>Nerities</i> sp. and <i>Phycosiphon</i> sp. Large scale deformation in the form of slumps and slide scars is often evident.</p>	<p>Interpretation: This massive, blocky, mudstone is interpreted to represent background hemipelagic sedimentation in the marine environment. This may occur in shelf to deep-water settings. Isolated silt- or sandstone lamina may represent the very distal fine tail of a turbidity current passing elsewhere in the basin. Deformation implies deposition on an often unstable slope, with remobilisation of gravitationally unstable sediment.</p>
---	---	---

1324

1325

Seismofacies	Amplitude & dimensions	Name and interpretation
	Low amplitude, low frequency, laterally continuous (where not truncated or deformed). Tens to hundreds of meters thick, but thousands to tens of thousands wide. Here observed within the thrust-cored anticlines and overlying seismofacies 4.	Background deposits. These are interpreted to represent background, mudstone dominated sediments deposited at a time when coarser grained sediments were not being delivered to the study area (sensu Vinnels et al., 2010).
	Alternating high and low amplitude, low frequency packages seen to be thickening towards the core of troughs and onlapping at margins. Seen within the trench-slope basins underlying seismofacies 4.	Ponded deposits. These are interpreted as alternating sandstone and mudstones ponding within heavily confined areas of the slope (Prather et al., 1998)
	Variable amplitude and frequency fill of lenticular incisions tens to hundreds of meters deep, by hundreds to thousands of meters wide, although typically less than 500 m wide.	Submarine channel fill. These incising features with variable fill are interpreted as submarine channel complexes (Mayall et al., 2010). These are seen to be conduits feeding both seismofacies 4 and 5 into the trench-slope basins.
	Mixed amplitude, low frequency radial, mounded features kilometres wide by tens of meters thick, stacking into packages hundreds of meters thick. Internally, reflectors may downlap towards the lateral margins and horizon slices display intricate high amplitude fingers radiating from the upstream portion of this unit.	Lobe complexes. These mounded, radial reflectors are interpreted as deep-marine lobe complexes (Booth et al., 2003). The high amplitude lenses are interpreted as distributary channels within the lobe complex, some of which are seen to extend beyond the high amplitude portions, implying bypass.
	Internally chaotic, irregular packages tens to hundreds of meters thick, often thousands of meters wide. Rarely coherent rafts or deformed packages of banded, high and low amplitude material can be seen internally.	MTDs. These chaotic geobodies are interpreted to represent MTDs (Posamentier and Kolla, 2003). These may be derived from the shelf or upper slope or local structures and may erode or block the system (Ortiz-Karpp et al., 2015).

1326

1327

Table 3. Examples of anomalously thick, aggradational lobe complex dimensions, bounding conditions and origin.					
System	Amalgamated lobe complex thickness	Age (temporal span)	Type of margin	Inferred control	Authority
Gres d'Annot, Chalufy, SE France (outcrop)	90 m	<30 Ma (Eocene – Oligocene)	Convergent, mini-basins	Sediment bypass in overfilled mini-basin	Joseph et al., 2000
Cervarola Sandstone, Italian Appenines (outcrop)	80 m, but generally not amalgamated	Miocene	Convergent, foredeep	Lateral structure growth	Tinetti and Piazza, 2019
Mahia Peninsula, New Zealand (outcrop)	385 m but intercalated with channel fill, MTDs and hemipelagites.	Late Miocene	Convergent, trench-slope basin	Migration of lobe complexes along axis of trench slope basin	Burgreen and Graham, 2014
Marnoso-Arenacea, Italian Appenines (outcrop)	20-40 m, but generally not amalgamated	Miocene	Convergent, foredeep	Increasing tectonic confinement	Tinetti and Tagliaferri, 2015
Southern Hikurangi Margin, New Zealand (outcrop and subsurface)	200 – 300 m	< 2 Ma	Convergent, trench-slope basin	Flow stripping over growing thrust structure	This study
Troika Field, Gulf of Mexico (subsurface)	80 - 200 m	Unknown	Passive, salt tectonics mini-basin	Flow stripping at salt evacuation structure	Horine et al., 2000
Active channel-mouth lobe complex, Congo-Angola margin (seafloor)	20-70 m	Present day	Passive margin	Sediment flux	Denniellou et al., 2017